AN ABSTRACT OF THE THESIS OF

HARI PRASAD GARG for the degree of DOCTOR OF PHILOSOPHY

in PHYSICS presented on June 12, 1975

Title: DETECTION AND ELECTRIC FIELD QUENCHING OF NITROGEN ATOMS IN THE $2s2p^3 3s\ ^6S_{5/2}$ METASTABLE AUTOIONIZING STATE

Abstract approved: _____

Dr. Clifford E. Fairchild

Nitrogen atoms in the $2s2p^3 3s\ ^6S_{5/2}$ state are predicted to have an energy greater than the lowest ionization energy of the atom. Atoms in this state are metastable against radiative transitions to lower states and also against Coulomb autoionization because of the selection rule $\Delta S = 0$ for both the processes, and can autoionize only through the magnetic interactions with the continuum. Because of the weakness of the magnetic interactions, nitrogen atoms in the $2s2p^3 3s\ ^6S_{5/2}$ state can have lifetimes of the order of microseconds, and therefore this state is described as metastable autoionizing state. In the present work nitrogen atoms in the $^6S_{5/2}$ metastable autoionizing state have been detected for the first time, using an atomic beam time-of-flight technique.

Since there is a possibility of spin flip by electron exchange in

electron-molecule collisions, dissociative excitation of N_2 molecules has been considered suitable to produce atoms in the $^6S_{5/2}$ metastable state. An atomic beam time-of-flight (TOF) apparatus with a flight path of 15.3 cm and a special detection device has been used to study and identify the dissociation fragments. Of the products of excitation and dissociation which travel towards the detector, charged particles are removed from the beam by using electric and magnetic fields. The neutral particles reaching the detector can be photons and metastable atoms and molecules. For photons, TOF $\cong$ 0; for the metastable atoms, a range of TOF associated with a mean kinetic energy of a few electron volts is obtained; and metastable molecules appear at very large TOF associated with thermal kinetic energies. Thus, it is not difficult to identify TOF spectrum due to metastable atoms.

In the present apparatus, the detector consists of copper target and a magnetic electron multiplier (MEM). The flight path of the particles from the source terminates on a copper wire and the MEM is arranged close to the Cu-wire and is biased to repel electrons and attract positive ions. Atoms in the metastable autoionizing states such as the $^6S_{5/2}$ state in nitrogen are readily ionized near the metal surface. Atoms in high-Rydberg states can also be ionized by surface ionization because their ionization energy is less than the electron work function of the metal surface. In this way, atoms in the ^4S ground state and ^2D and ^2P metastable states are not detected by the

detector, and the metastable atomic TOF spectrum can be due only to atoms in the $^6S_{5/2}$ metastable state and Rydberg states. A positive identification of atoms in the $^6S_{5/2}$ metastable state is obtained by making use of the unique way in which Rydberg-state atoms are quenched in a dc electric field.

The electric field dependent decay constant, $\gamma(E)$, for the $^6S_{5/2}$ metastable nitrogen atoms is measured and its functional dependence on E has been determined. Whereas the first order perturbation theory gives $\gamma(E) \propto E^2$, experimentally it is found that the data best satisfy a linear relation between $\gamma(E)$ and E, i.e., $\gamma(E) = kE$, where experimentally, $k = (6.4 \pm .5) \times 10^4$ sec^{-1}/(kV/cm). Because of the linear dependence of $\gamma(E)$ on E and the ease with which the atoms in the $^6S_{5/2}$ metastable state are quenched in the electric field, the quenching is regarded as anomalous.

A tentative explanation of the anomalous quenching in an external dc electric field of atoms in the $^6S_{5/2}$ metastable autoionizing state is obtained by considering the mixing of $^6S_{5/2}$ wave function of the $2s^2 2p^2(^1D)n\ell$ Rydberg states. This mixing allows the state to be quenched by a field ionization effect and thereby provides a mechanism for rapid decay. It is also proposed that instead of lying at 17.2 eV above the ground state as predicted earlier, the $^6S_{5/2}$ metastable state is nearly degenerate with the $2s^2 2p^2(^1D)$ metastable state of N^+ ion.

Detection and Electric Field Quenching of Nitrogen Atoms in the $2s2p^3 3s\ ^6S_{5/2}$ Metastable Autoionizing State

by

Hari Prasad Garg

A THESIS

submitted to

Oregon State University

in partial fulfillment of
the requirements for the
degree of

Doctor of Philosophy

Completed June 12, 1975

Commencement June 1976

APPROVED:

Redacted for privacy

Associate Professor of Physics
in charge of major

Redacted for privacy

Chairman of Department of Physics

Redacted for privacy

Dean of Graduate School

Date thesis is presented June 12, 1975

Typed by Suelynn Williams for Hari Prasad Garg

ACKNOWLEDGEMENTS

I welcome this opportunity to express gratitude to my major professor, Dr. Clifford E. Fairchild, for his guidance, help and encouragement during the course of this investigation.

I am greatly indebted to Dr. Carl A. Kocher for many helpful discussions over a period of two years and proofreading the manuscript.

I thank Professors Victor A. Madsen, Charles Drake and Roman C. Schmitt for their suggestions and serving on my graduate advisory committee.

My thanks go to Professor Larry Schecter, Chairman, for encouragement and providing research facilities, to Dr. Jerris Johnson for help in computer programming and to the O.S.U. Computer Center for awarding a computer grant for data analysis.

Finally, My wife, Shanti, deserves special thanks for her moral support, patience and encouragement.

TABLE OF CONTENTS

LIST OF FIGURES

LIST OF TABLES

DETECTION AND ELECTRIC FIELD QUENCHING OF NITROGEN ATOMS IN THE $2s2p^3 3s\ ^6S_{5/2}$ METASTABLE AUTOIONIZING STATE

1. INTRODUCTION

At present there is considerable interest in the study of autoionizing and metastable autoionizing states in various elements (1-8). The present work is concerned with the detection of nitrogen atoms in the $2s2p^3 3s\ ^6S_{5/2}$ metastable autoionizing state and their quenching in a dc electric field. To date it has not been possible to observe nitrogen atoms in the $^6S_{5/2}$ state spectroscopically (9-11). Innes and Oldenberg (12, 13) first proposed that nitrogen atoms in the $^6S_{5/2}$ state must be taking part in the auroral afterglow and be metastable and highly energetic. Prag and Clark (14, 15) also proposed a mechanism involving atoms in the $^6S_{5/2}$ state for the auroral afterglow, and, by the extrapolation method for isoelectronic atoms, predicted the energy level of the $^6S_{5/2}$ state to be at 17.2 eV. At this energy the $^6S_{5/2}$ state would lie in the ionization continuum, since the first and second ionization limits of nitrogen are known (11) to lie at 14.5 and 16.43 eV respectively. Since the $^6S_{5/2}$ state is predicted to lie in the ionization continuum and to be metastable, an effort is made below to explain the phenomenon of autoionization (16-19) and metastable autoionizing states.

1.1 Autoionization

Discrete atomic states which have energies greater than the first atomic ionization energy are known as autoionizing states. Whereas some of these states can decay radiatively by allowed transistions to lower bound states, all of these states may also make spontaneous radiationless transitions to a continuum state (consisting of a singly ionized atom and a free electron) of the same energy. This phenomenon is known as autoionization. It is represented by the reaction

$$A^* \rightarrow A^+ + e + K.E. \quad , \qquad 1.1$$

where A^* is the atom in an autoionizing state, A^+ is the singly ionized atom, e is the outgoing electron, and K.E. is the kinetic energy shared by the ion and the electron and is equal to the difference in the energies of the A^* atom and A^+ ion.

To describe autoionization, an initial state is defined as a fictitious rigorously bound stable discrete state ψ_d which is formed by neglecting those (or all) terms in the Hamiltonian which lead to configuration mixing (16). According to time-dependent perturbation theory (20), the first order rate for a transition from this discrete state with energy E_d to a continuum state ψ_c of energy E_c is given by

$$w^{(1)} = \frac{2\pi}{\hbar} \left| \langle \psi_c | H' | \psi_d \rangle \right|^2 \delta(E_c - E_d) \qquad 1.2$$

where H' is the perturbation coupling the discrete and continuum states, and, in general, represents all the non-central terms in the complete Hamiltonian for the atom. In Eq. 1.2, the factor $\delta(E_c - E_d)$ represents a zero transition rate to states of energy other than $E_c = E_d$. In other words, these transitions conserve energy. In a case where the first-order matrix element vanishes, the second-order transition rate is given by

$$w^{(2)} = \frac{2\pi}{\hbar} \left| \sum_i \frac{\langle \psi_c | H' | \psi_i \rangle \langle \psi_i | H' | \psi_d \rangle}{E_d - E_c} \right|^2 \delta(E_c - E_d) \quad , \qquad 1.3$$

where the summation is over all intermediate states ψ_i.

Autoionizing states can be of two types:

(1) The first are the kind that are coupled very strongly to the adjacent continuum through the repulsive electrostatic terms ($H' = \sum_{i<j} \frac{e^2}{r_{ij}}$) in the Hamiltonian. These are called Coulomb autoionizing states and have very short lifetimes, typically of the order of 10^{-12} - 10^{-15} sec (3-6).

(2) Autoionizing states of the second type are those which are coupled only weakly to the adjacent continuum through magnetic terms in the Hamiltonian (i.e. spin-orbit, spin-other-orbit and spin-spin interactions). Because of the weakness of the magnetic

interactions, these states are metastable against autoionization and have autoionizing lifetimes of the order of 10^{-3} to 10^{-7} sec (1-4). Such states are called metastable autoionizing states.

The continuum state ψ_c is described in the same manner as the discrete state, by specifying the spin and orbital angular momentum quantum numbers for the state of the resulting ion and free electron. The free electron, although moving in an open orbit, has a definite orbital angular momentum with respect to the center of mass of the system. The total angular momentum of the continuum is the sum of the angular momenta of the outgoing electron and the residual ion. The parity of the state is defined as either even or odd according to whether $\sum_i \ell_i$ is even or odd, where the sum is taken over all electrons.

The selection rules and the estimated relative transition rates for autoionization (based on L-S coupling) via the electrostatic and various magnetic interactions are shown in Table I (1, 21).

In Table I, α is the Sommerfeld fine-structure constant, m is the mass of the electron and M is the proton mass. The relative decay rates are evaluated by assuming that all electronic distances are of the order of a Bohr radius. It is noteworthy that the transition rates for magnetic interactions are of the order of α^4 times the transition rate for Coulomb autoionization; therefore, as noted above,

Table I. Selection Rules for Autoionization

Interaction	ΔL	ΔS	ΔJ	Parity Change	Relative Transition Rate
Coulomb	0	0	0	No	1
Spin-Orbit, Spin-Other-Orbit	$0, \pm 1$	$0, \pm 1$	0	No	α^4
Spin-Spin	$0, \pm 1, \pm 2$	$0, \pm 1, \pm 2$	0	No	α^4
Hyperfine	$0, \pm 1, \pm 2$	$0, \pm 1, \pm 2$	$0, \pm 1$	No	$\alpha^4 (m/M)^2$

autoionizing states which decay only via magnetic interactions are metastable, with lifetimes which are expected to be of the order of 10^{-4} - 10^{-7} sec. These lifetimes are long compared to typical radiative lifetimes so that a state will be truly long lived only if it is also metastable against radiative transitions to lower lying levels.

Since the Coulomb and all but one (spin-orbit) of the magnetic interactions are two-electron operators, generally a two electron transition is involved in the autoionization process. For example, in He the lowest lying autoionizing configuration is $2s^2$ and its autoionizing transition is described by the process

$$2s^2 \rightarrow 1sks \ ,$$

where k represents the wavenumber of the outgoing electron.

All of these theoretical considerations will be used in the study of metastable autoionizing states in nitrogen.

1.2 Metastable Autoionizing States in Nitrogen

A partial term diagram of nitrogen, relevant to the phenomenon of autoionization, is shown in Fig. 1. The lowest electronic configuration of the nitrogen atom ($1s^2 2s^2 2p^3$) gives rise to three states, the ground state $^4S^o_{3/2}$, and the $^2D^o$ and $^2P^o$ metastable states, which lie at energies of 2.38 eV and 3.57 eV respectively (10, 11). (The superscript "o" indicates the odd parity of the states and will not be indicated in the rest of the text unless it is important for clarification.) Thus the lowest electronic configuration for nitrogen consists of quartet and doublet terms. By the excitation of one of the $2p^3$ electrons into higher quantum states, radiating bound states of quartet and doublet multiplicities are obtained. These excited states are responsible for the normal atomic spectrum of nitrogen, denoted by I or I^a spectra. Removal of one of the 2p electrons from the atom results in the $2p^2$ configuration of the N^+ ion, which has three terms, ^3P, ^1D and ^1S. Therefore nitrogen will have three ionization potentials corresponding to the $2p^2$ ionic parentage. The first and lowest ionization potential is at 14.54 eV for ^3P state of the ion, and 16.43 eV and 18.59 eV corresponding to ^1D and ^1S states respectively. The ionization continuum of the nitrogen atom is therefore composed of

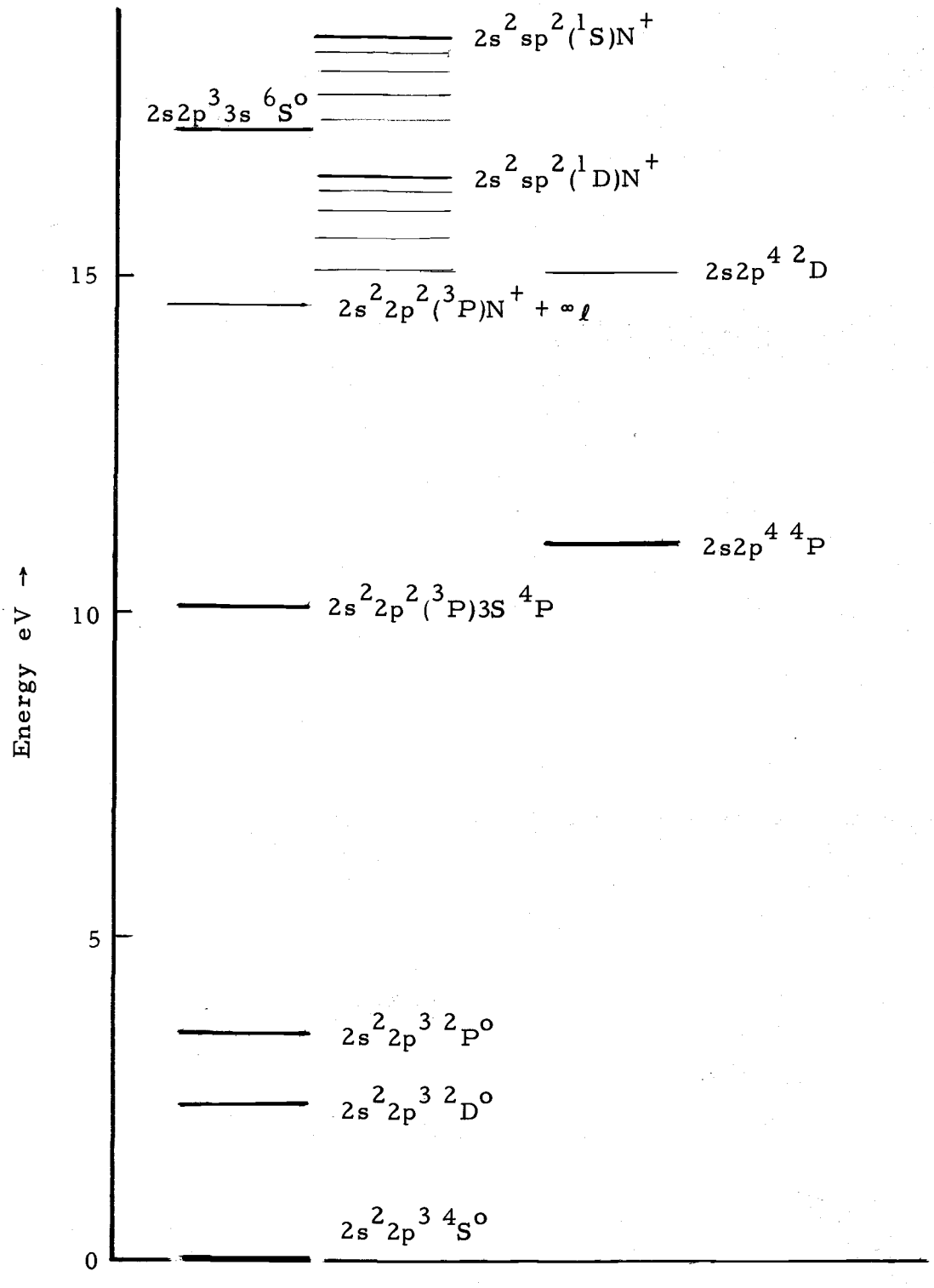

Fig. 1. Partial term diagram of nitrogen.

quartet and doublet states. By the excitation of one of the electrons from the outermost filled shell, $2s^2$, states are obtained which give rise to the spectrum designated by I^b (9, p. 161). The lowest of these configurations is $2s2p^4$, giving rise to ^4P, ^2P, ^2D and ^2S terms, of which only the ^4P is known. This multiplet has been observed spectroscopically and lies at 10.91 eV above the ground state. The term $2s2p^4\ ^2D$ is predicted (5) to be an autoionizing state, with an excitation energy of 14.9 eV. The next lowest configuration is $2s2p^3 3s$, which gives rise to $^6S^o$, $^4S^o$, $^4D^o$, $^2D^o$, $^4P^o$ and $^2P^o$ terms. Of these, the $^6S^o_{5/2}$ state will lie lowest, and, as noted previously, it is predicted to lie in the first ionization continuum, at 17.2 eV above ground state. Other states $^4S^o$, $^4D^o$, $^2D^o$, $^4P^o$ and $^2P^o$ will be of higher energy than that of $^6S^o$, and they are autoionizing via the Coulomb interaction, as shown below:

$$(2s2p^3 3s)\ {}^4S^o_{3/2} \xrightarrow{\text{Coul.}} (2s^2 2p^2\ {}^3P\ N^+ + kp)\ {}^4S^o_{3/2}$$

$$^4D^o_J,\ ^2D^o_J \xrightarrow{\text{Coul.}} (2s^2 2p^2\ {}^3P\ N^+ + kp)\ {}^4D^o_J,\ {}^2D^o_J$$

$$^4D^o_J,\ ^2D^o_J \xrightarrow{\text{Coul.}} (2s^2 2p^2\ {}^3P\ N^+ + kf)\ {}^4D^o_J,\ {}^2D^o_J$$

$$^4P^o_J,\ ^2P^o_J \xrightarrow{\text{Coul.}} (2s^2 2p^2\ {}^3P\ N^+ + kp)\ {}^4P^o_J,\ {}^2P^o_J$$

In these decay reactions k denotes the wave number of the ejected

free electron.

The $2s2p^3 3s\ ^6S^o_{5/2}$ state does not satisfy the $\Delta S = 0$ selection rule for Coulomb autoionization, and is therefore metastable with respect to this process. Since there are no sextet terms in the I^a term sequence, the $2s2p^3 3s\ ^6S^o_{5/2}$ state is also metastable against radiation, and it is the ground state of the sextet system. The $^6S^o_{5/2}$ state can decay to the continuum through magnetic terms in the Hamiltonian, i.e. Spin-Orbit, Spin-Other-Orbit and Spin-Spin interactions. Also, the $^6S^o_{5/2}$ state can couple to the continuum in second order through rapidly autoionizing $2s2p^3 3s\ ^4D^o_{5/2}, ^2D^o_{5/2}, ^4P^o_{5/2}$ states of the same configuration by the same magnetic interactions as follows:

$$(2s2p^3 3s)\ ^6S^o_{5/2} \xrightarrow{\text{Spin-Spin}} (2s2p^3 3s)\ ^4D^o_{5/2},\ ^2D^o_{5/2}$$

$$\xrightarrow{\text{Spin-Orbit}} (2s2p^3 3s)\ ^4P^o_{5/2}$$

There are three terms ^3P, ^1D and ^1S of $2s^2 2p^2\ N^+$ ion, and as is clear from Fig. 1, the $^6S_{5/2}$ state lies in the continuum of only two of them i.e. $(2s^2 2p^2\ ^3P\ N^+ + k\ell)$ and $(2s^2 2p^2\ ^1D\ N^+ + k\ell)$. The $^6S_{5/2}$ state does not couple with $2s^2 2p^2\ (^1S)n\ell$ Rydberg states through any of the interactions mentioned i.e. Coulomb, S-O, S-O-O, S-S, or even through a radiative transition. It can of course couple via magnetic interactions with the continua as follows:

$$2s2p^3 3s\ {}^6S^o_{5/2} \xrightarrow{\text{S-S}} (2s^2 2p^2\ {}^1D\ N^+ + kp)\ {}^2D^o_{5/2}$$

$$\xrightarrow{\text{S-S}} (2s^2 2p^2\ {}^1D\ N^+ + kf)\ {}^2D^o_{5/2}$$

$$\xrightarrow{\text{S-O and S-S}} (2s^2 2p^2\ {}^3P\ N^+ + kp)\ {}^4P^o_{5/2},\ {}^4D^o_{5/2}$$

$$\xrightarrow{\text{S-S}} (2s^2 2p^2\ {}^3P\ N^+ + kp)\ {}^2D^o_{5/2}$$

$$\xrightarrow{\text{S-O, S-S}} (2s^2 2p^2\ {}^3P\ N^+ + kf)\ {}^4D^o_{5/2}$$

$$\xrightarrow{\text{S-S}} (2s^2 2p^2\ {}^3P\ N^+ + kf)\ {}^2D^o_{5/2}$$

Other sextets can be obtained from configurations such as $2s2p^3 3p\ {}^6P_J$. These can decay radiatively to $2s2p^3 3s\ {}^6S^o_{5/2}$ and will therefore not be metastable.

It is obvious from the above discussion that the $2s2p^3 3s\ {}^6S_{5/2}$ state for nitrogen atoms is predicted to be a metastable autoionizing state, with a natural lifetime of the order of 10^{-7} to 10^{-4} sec. Nitrogen atoms in the $2s2p^3 3s\ {}^6S_{5/2}$ state have not been seen spectroscopically. Feldman and Novick (35) reported the possible existence of nitrogen atoms in the $2s2p^3 3s\ {}^6S_{5/2}$ state in a laboratory experiment by bombarding N_2 molecules with electrons. The excitation threshold was observed to be 30 eV, which they accounted for by

allowing 9.8 eV for dissociation and 20 eV for $N(^6S)$ atoms in the center-of-mass system. They also reported having observed the quenching of the signal of the metastable atoms by both electric and magnetic fields. In the present experiment, on the basis of both the quenching of metastable atoms in the electric field and the lifetime measurement, it is concluded that nitrogen atoms in $2s2p^3 3s\ ^6S_{5/2}$ state have been detected using an atomic beam time-of-flight technique.

2. THE EXPERIMENTAL METHOD

2.1 Production of Nitrogen Atoms in the $2s2p^3 3s\ ^6S_{5/2}$ State

Dissociation of molecules by electron bombardment has been widely used as a means of producing metastable atoms (22, 24, 41). One can also produce metastable excited atoms by bombarding atoms in the ground state with electrons or other projectiles. Recently (7), the $2s2p^3np\ ^4P$ autoionizing states of nitrogen have been studied by photoionization of ^4S ground state nitrogen atoms. Of course this latest method of photoionization cannot be used for producing $^6S_{5/2}$ nitrogen atoms because of the selection rule $\Delta S = 0$ for electric dipole transitions. It is considered unnecessary to first produce the nitrogen atoms in the ^4S ground state and then excite them to the metastable $^6S_{5/2}$ state by electron collision. Therefore, in the present experiment, metastable nitrogen atoms in $^6S_{5/2}$ state are produced directly in dissociative excitation, by electron impact on N_2 molecules. Figure 2 shows schematically the molecular potential curves (23) for the nitrogen molecule which are important for illustrating the mechanism of dissociative excitation.

The two potential curves associated with a ground state atom and an atom in the $2s2p^3 3s\ ^6S_{5/2}$ metastable autoionizing state are labelled "tentative" because their structure has not been calculated. The first experimental data indicative of their structure is presented

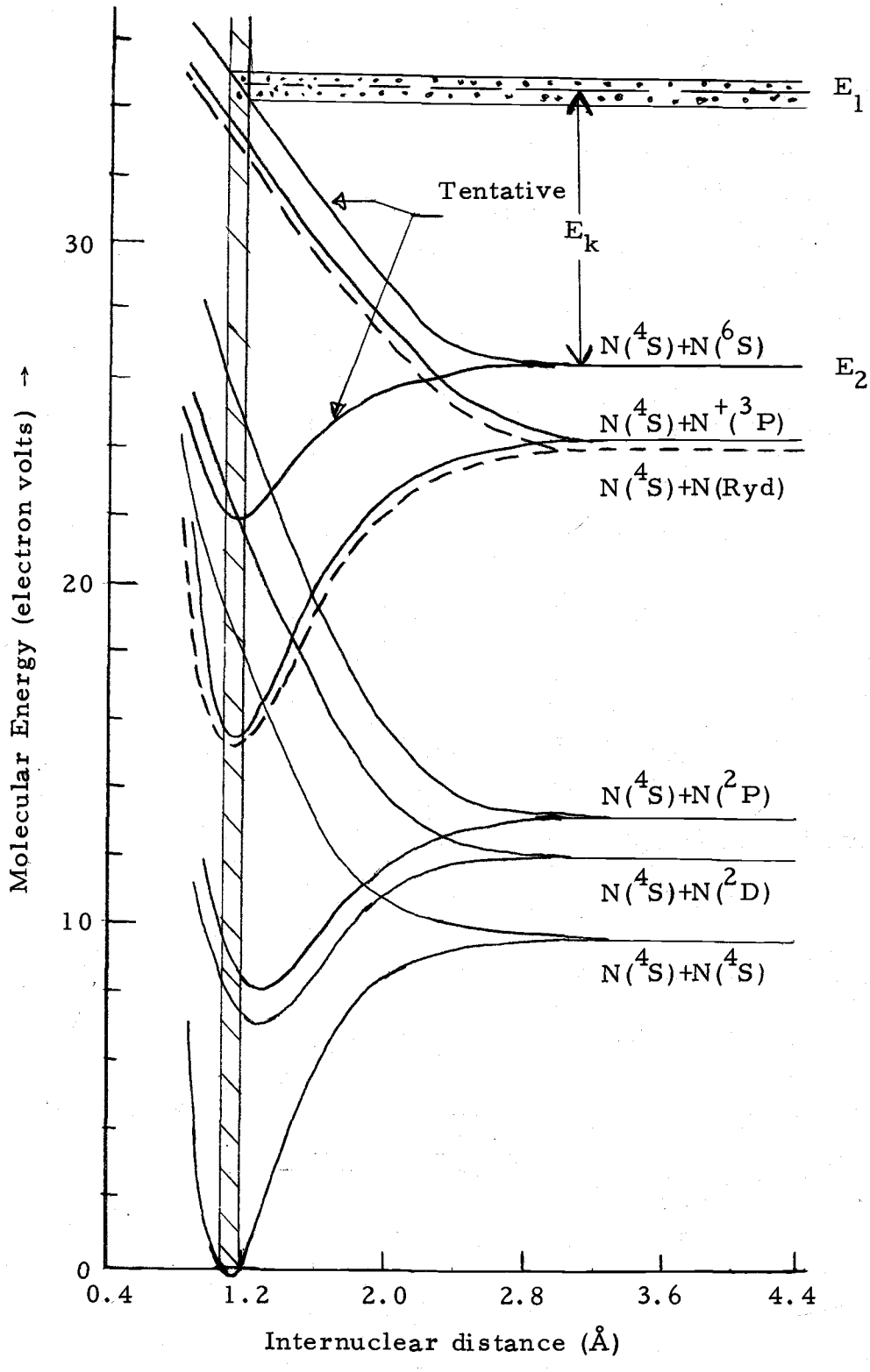

Fig. 2. Molecular potential curves for N_2 and N_2^+ relevant for obtaining metastable atoms by dissociative excitation by electron bombardment of N_2 molecule.

in the present work, as described in Chapter 4.

Close to the lowest lying potential curve of N_2^+ (which has the states $N(^4S)$ and $N^+(^3P)$ as its dissociation limit) and almost parallel to it will be the potential curves of a neutral molecule with one atom in the ^4S ground state and the other one in long-lived highly excited state, i.e., a Rydberg state (24). These potential curves are represented by the dashed lines in the figure. Since atoms in Rydberg states are often an important product of dissociative excitation, their properties will be reviewed here.

Atoms in Rydberg states are those which have at least one electron with large principal quantum number. They are not metastable by any selection rule, but can have long enough lifetimes to be observed in atomic beam experiments. For a hydrogen atom, the theory of high-Rydberg states gives the following properties (24):

(i) Binding energy $= \frac{13.6}{n^2}$ eV, where n is the principal quantum number.

(ii) Mean value of radius $= n^2 a_o$, where a_o is the Bohr radius.

(iii) Radiative lifetime (for a given angular momentum state) $\propto n^3$.

For n = 20, the binding energy is only 0.034 eV, and the mean radius is of the order of 200 Å, which is huge for an atom. Also, the radiative lifetime varies from 1.6 μsec for $\ell = 1$ to 100 μsec for

ℓ = 19 (24, 26). Therefore a significant fraction of these atoms might reach the detector of a typical time-of-flight apparatus (See Fig.3, page 21). Nitrogen atoms in Rydberg states are expected to have similar properties (22, 24).

To be complete, Fig. 2 should display many additional molecular potential curves, but only a few, enough to explain the mechanism of dissociation by electron bombardment are shown. When an energetic electron bombards a molecule in the ground state the molecule is excited to a state represented by either a bound or a repulsive potential curve. As described by the Franck-Condon principle, excitation takes place vertically in the shaded region (the Franck-Condon region) shown in Fig. 2. The kinetic energy E_k shared by the dissociation fragments is the difference between the excitation energy E_1 and the potential energy E_2 of the dissociation fragments at infinite separation and is also shown in Fig. 2. Excitation to a repulsive potential curve, as shown in Fig. 2, is not the only mechanism for dissociation of a molecule. Excitation to the repulsive wall of a bound potential at an energy larger than the dissociation limit can also result in the dissociation of the molecule as can predissociation. In practice, all the above three processes can be responsible for the dissociation.

Dissociation occurs during roughly $\frac{1}{2}$ of a vibrational period, approximately 10^{-13} sec, and the two atoms in the center-of-mass

frame fly apart in opposite directions. Using conservation of momentum in center-of-mass system, we obtain that for homonuclear diatomic molecules, such as N_2, the kinetic energy E_k will be equally shared by the two atomic fragments, even if one atom is in the ground state and the other one is in an excited state. Thus, we can write

$$E_{k1} = E_{k2} = \tfrac{1}{2} E_k \, . \qquad 2.1$$

Since the electron impact may produce the upper state at any internuclear distance in the Franck-Condon region, fragments are formed with a range of translational energies, as shown by the dotted region in Fig. 2, and the kinetic energy distribution of fragments will depend on the shape of molecular potential curve as well as on the mechanism for dissociation (dissociation by excitation to a repulsive molecular potential curve, dissociation by excitation to the repulsive wall of a bound potential curve, or predissociation). If these fragments travel a fixed distance between a point of production and a detector, they will accordingly have a range of times-of-flight, and they will exhibit a time-of-flight (TOF) distribution or spectrum. The kinetic energy distribution, the velocity distribution and TOF distribution of fragments are related to each other and are interconvertible. If L is the length of flight path, t is the time of flight, and m is the mass of the atom, then we have the following relations:

$$v = \frac{L}{t}, \qquad dv = -\frac{L}{t^2}\,dt, \qquad \frac{dt}{dv} = -\frac{t^2}{L},$$

$$E = \tfrac{1}{2}mv^2 = \tfrac{1}{2}m\frac{L^2}{t^2}, \qquad dE = -\frac{mL^2}{t^3}\,dt, \qquad \frac{dt}{dE} = -\frac{t^3}{mL^2},$$

$$P(E)\,dE = P(v)\,dv = P(t)\,dt,$$

$$P(E) = P(t)\left|\frac{dt}{dE}\right| = \frac{t^3}{mL^2}\,P(t), \tag{2.2}$$

and $$P(v) = P(t)\left|\frac{dt}{dv}\right| = \frac{t^2}{L}\,P(t), \tag{2.3}$$

where $P(E)$, $P(v)$ and $P(t)$ represent distributions in kinetic energy, velocity and time-of-flight respectively at the detector. Because of the natural decay of the fragments along the flight path, the TOF distribution at the detector $P(t)$ is not the same as that at the source. If the fragments are in a single metastable state with single decay constant γ, the TOF distribution at the detector $P(t)$ is related to the TOF distribution at the source $P_s(t)$ by the relation

$$P(t) = P_s(t)\,e^{-\gamma t}.$$

Therefore,

$$P_s(E) = \frac{t^3}{mL^2}P_s(t) = \frac{t^3}{mL^2}e^{\gamma t}\,P(t) = e^{\gamma t}\,P(E), \tag{2.4}$$

where $P_s(E)$ is the kinetic energy distribution of fragments at the source. If TOF analysis is to be used to study the shape of the

molecular potential curves, $P_s(E)$ is the desired quantity. As will be shown in detail in the following paragraphs, time-of-flight analysis can be used to provide a very sensitive and unambiguous method for the detection and identification of metastable atoms produced by dissociative excitation.

Typically, a particle detector which is sensitive to metastable atoms, will also be an efficient detector for photons, metastable molecules and positively or negatively charged particles; and additionally, the many processes by which these particles can be produced will typically compete efficiently with dissociative excitation. For example, if N_2 molecules are bombarded with electrons having a kinetic energy of 30 eV, there are a number of important processes which occur:

1. Excitation to metastable states of the molecule

$$e + N_2 \rightarrow e' + \begin{Bmatrix} N_2^R \\ N_2^m \end{Bmatrix} ,$$

where N_2^R and N_2^m represent molecules in long-lived Rydberg states, and in all other metastable states, respectively.

2. Excitation to molecular states which decay by allowed radiative transitions

$$e + N_2 \rightarrow e' + N_2^* ,$$

followed by $N_2^* \rightarrow N_2 + h\nu$.

3. Ionization of the molecule

$$e + N_2 \rightarrow N_2^+ + e' + e''$$

4. Dissociative excitation producing metastable atoms

$$e + N_2 \rightarrow e' + N + \left\{ \begin{matrix} N^R \\ N^m \end{matrix} \right\},$$

where N^R and N^m represent atoms in long-lived Rydberg states, and in all other metastable states, respectively.

5. Dissociative excitation to atoms in short-lived radiative states

$$e + N_2 \rightarrow e' + N + N^*,$$

followed by $N^* \rightarrow N + h\nu$

6. Dissociative ionization

$$e + N_2 \rightarrow N + N^+ + e' + e'' .$$

Although the charged particles emanating from the point of production associated with a pulse of excitation can be deflected and collected using static electric and magnetic fields, photons and metastable molecules can travel the same path as the metastable atoms. Additionally, in a typical situation the number of photons and metastable molecules produced during and immediately after an excitation

pulse will be much larger than the number of metastable atoms. However, generally speaking, the different types of neutral particles fall into three widely separated regions of TOF. For nearly all the photons, TOF $\simeq$ 0; for the metastable atoms, a range of TOF associated with a mean kinetic energy of a few electron volts is obtained; and the metastable molecules appear only at very large values of TOF, associated with thermal kinetic energies. These ideas are illustrated qualitatively in a typical TOF spectrum shown in Fig. 3. The excitation pulse for this TOF spectrum has a duration of 0.4 μsec, and the spectrum shown would be accumulated by a detector located approximately 15 cm from the point of excitation. Thus TOF analysis is clearly useful in identifying the different types of neutral particles.

The entire TOF spectrum associated with a given molecular potential curve cannot be obtained unless the energy of the bombarding electrons is somewhat larger than the threshold energy for dissociative excitation (See Fig. 2 and its discussion). However, for bombarding energies larger than that required to obtain the complete TOF spectrum, the shape of the spectrum is nearly independent of the bombarding energy. This feature of the dissociative excitation process allows use of bombarding energies much larger than the threshold energy, in an energy range where the efficiency for the process is greatest.

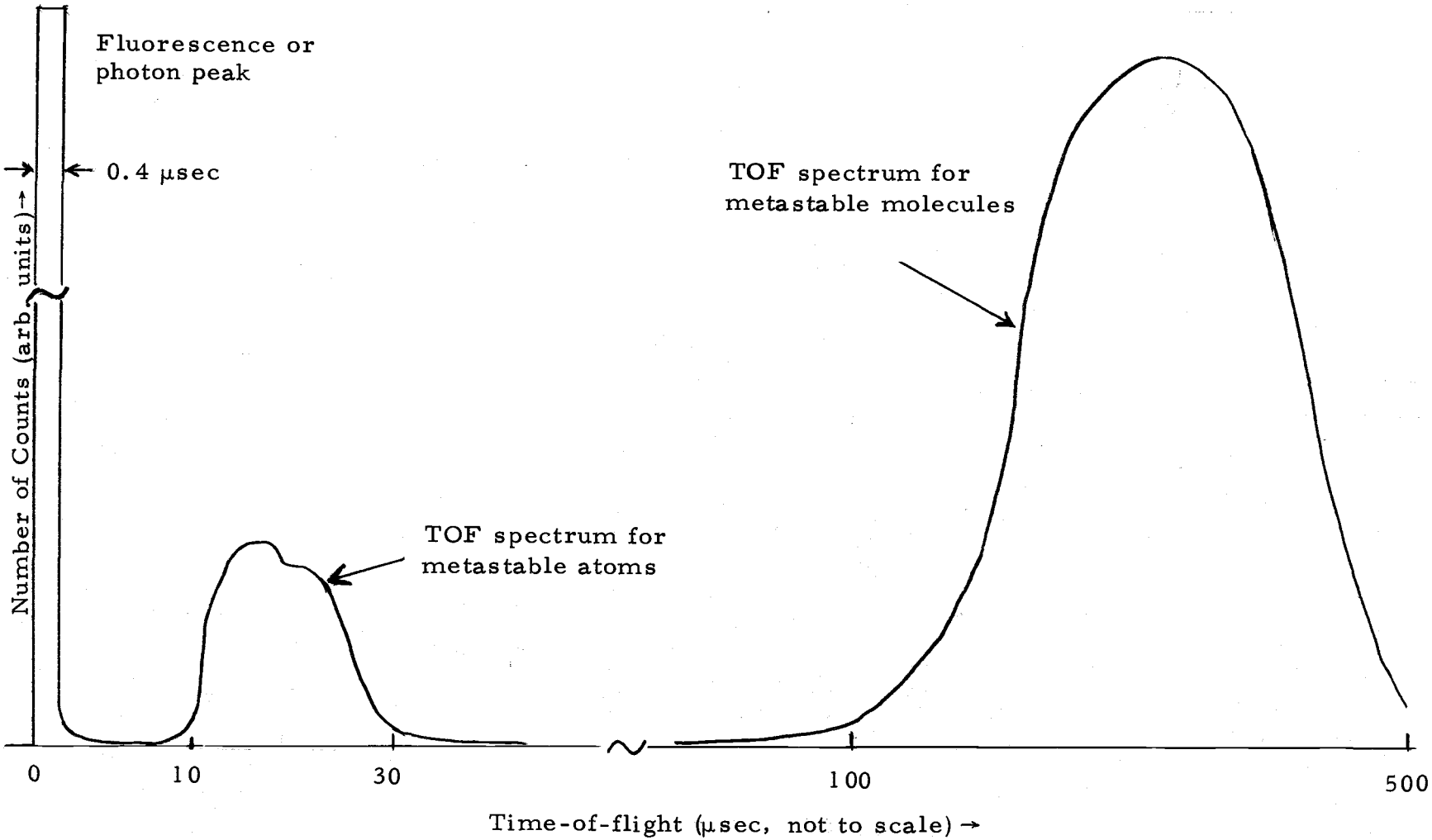

Fig. 3. Illustration of time-of-flight spectra of photons and metastable atoms and molecules from electron gun to detector, for a typical experimental situation, approximate flight path = 15 cm; pulse width = 0.4 μsec.

2.2 The Time-of-Flight Technique

A typical TOF apparatus is shown schematically in Fig. 4. The target, consisting of gas molecules in the electron gun region, is bombarded by a short burst of electrons at time t = 0. When a molecule dissociates, the fragment atoms can fly in any direction, and some of them will travel in a direction defined by the two slits shown in Fig. 4. These slits define a flight path between the electron bombardment region (the electron gun) and the detector. The fragment atoms together with photons and metastable molecules, are detected by a detector at a distance L at various later times t. The time-of-flight is measured using a standard timing technique. The START pulse to a time-to-pulse-height converter (TPHC, also called a time-to-amplitude converter or TAC) is synchronized with the electron gun pulse, and the STOP input to the TAC is activated by a pulse from the detector, as indicated in Fig. 4. The height of a given output pulse of the TAC is proportional to the time between the corresponding START and STOP pulses, and these output pulses are conveniently stored in a multi-channel pulse height analyzer. A TOF spectrum is accumulated by regular repetition of the electron gun pulses. The TAC can record only one pulse per cycle of operation. Once the charging ramp of TAC is stopped by a pulse from the detector, the TAC becomes dead for the remaining part of the cycle

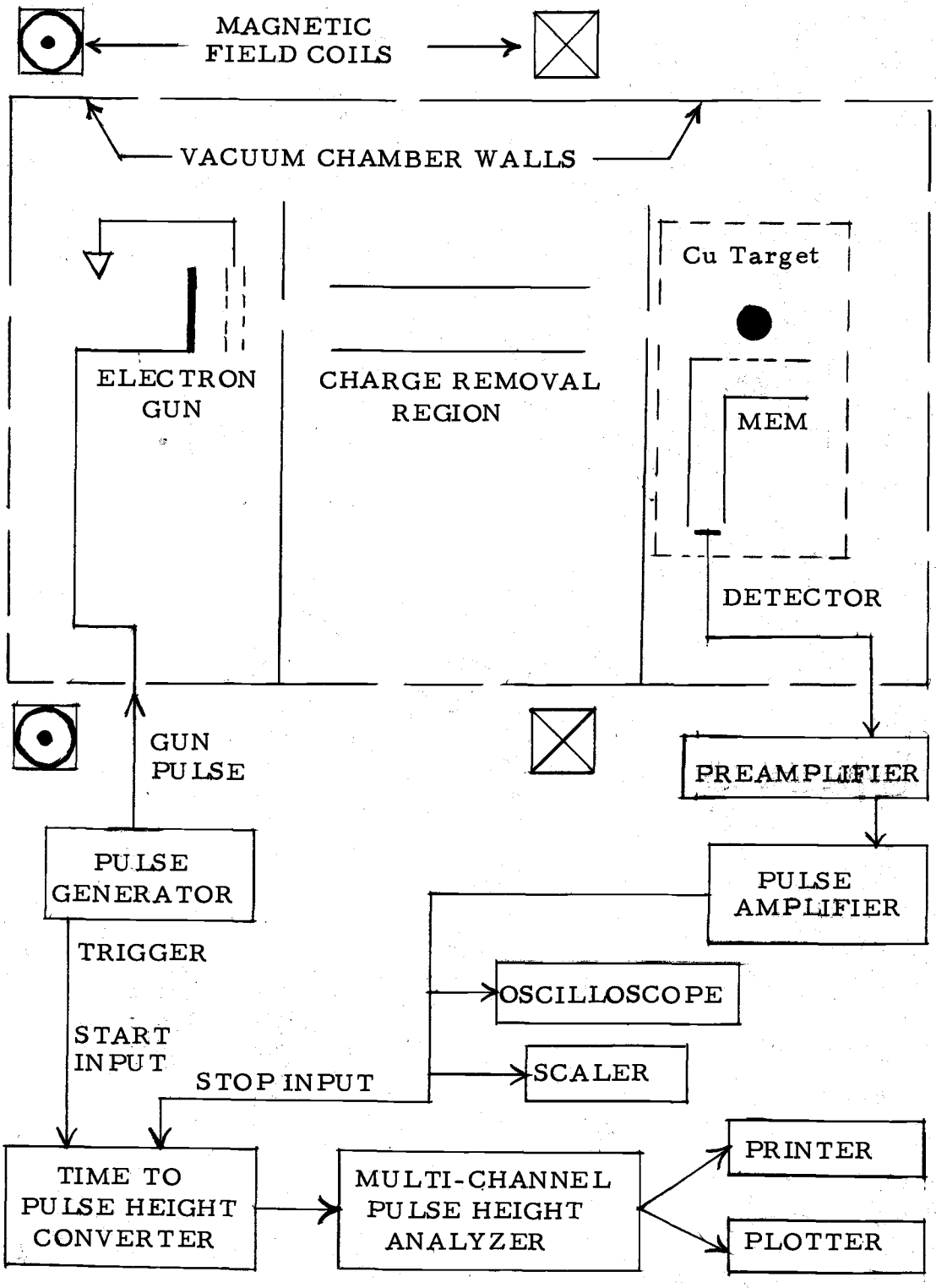

Fig. 4. Schematic diagram of the apparatus.

and any more pulses from the detector will not be recorded. Thus the over-all count rate can never be larger than the repetition rate of the excitation pulses. Since photons are the earliest to arrive at the detector, and, if for each excitation pulse a photon is detected, only a photon TOF spectrum will be accumulated, i.e., metastable atoms or molecules will not be detected. Thus, it is noteworthy that in order to obtain a TOF spectrum which is not distorted by the effects of the dead time of the TAC, the total count rate must be low enough that the probability for the occurrence of more than one detector pulse per cycle of operation is negligible. In the present experiment the maximum repetition rate is limited by the long flight times of metastable molecules, and the count rate is always much smaller than the repetition rate.

2.3 Detection Scheme

By using TOF analysis together with weak electric and magnetic fields for charge confinement and remvoal (See Fig. 4), a TOF spectrum for a beam of atoms produced by dissociative excitation can be readily identified and isolated (See Fig. 3). However, there are two additional features of these types of time-of-flight spectra, i.e., those associated with the dissociative excitation processes, which create a need for using a very special detection scheme (particle detector plus auxiliary devices). First, there is a contamination of

the TOF spectrum by photons emitted by metastable atoms and molecules as they travel along the flight path. For example, a photon emitted by a slow molecule, near the beginning of the flight path, might reach the detector at the same TOF as that of a fast atom. Although these photons are emitted randomly in all directions, their effects can be significant. They can even cause spurious peaks in a TOF spectrum, because of solid angle effects associated with the peculiarities of the flight path geometry.

The second feature of the TOF spectrum which creates a need for a complicated detection scheme is that the dissociative molecular potential curves associated with different pairs of atomic states are all very similar (See Fig. 2). Since the detailed structure of many of these curves is not precisely known, TOF analysis generally cannot be used to provide for separate identification of atoms in different metastable states. For example, it can be seen from Fig. 2 that production of nitrogen atoms in the $2s2p^3 3s\ ^6S_{5/2}$ metastable autoionizing state by electron impact dissociation of N_2 is necessarily accompanied by the production of nitrogen atoms in the ^4S ground state as well as in the $2p^3\ ^2D$ and $2p^3\ ^2P$ metastable states, and in long-lived high-Rydberg states. It is also evident from Fig. 2 that all these long lived atoms will have similar or nearly identical TOF spectra. Therefore, an over-all detection scheme (a detector plus auxiliary devices) which can identify atomic states is required.

It is fortunate that the detection scheme which serves to provide the minimum efficiency for the detection of photons also provides discrimination against neutral atoms in low-lying metastable states. As is indicated in Fig. 4, the particle detection process is initiated at a metal target which terminates the atomic beam flight path. The desired discrimination is then obtained by locating an electron multiplier (labelled MEM in Fig. 4) near the target and biasing the multiplier to detect positive ions. Thus, any electrons released at the metal target are repelled by the electron multiplier, and positive ions are attracted toward it. This procedure provides the desired discrimination because photons and atoms in low-lying metastable states which strike the target can only be reflected or cause the emission of Auger electrons. In contrast, an atom in a metastable autoionizing state is readily ionized near the surface of the target, and the resultant ion is then accelerated toward the cathode of the electron multiplier.

In general, positive ions can also be produced at a surface by surface ionization (27–29), which can be represented by the process

$$P^* + M \rightarrow P^+ + M^- \qquad 2.5$$

where P^* represents a metastable atom or molecule and M represents a metallic surface. Neglecting the initial kinetic energy of P^*, the approximate threshold condition for surface ionization is that the

ionization energy of P^* must be less than the electron work function of the surface. The consideration of this type of surface ionization must be included here because, as has been mentioned, the atomic beam may contain atoms in Rydberg states, which can be ionized by surface ionization.

In summary, the present detection scheme provides an extremely low efficiency for the detection of photons and atoms in low-lying metastable states, it may have an appreciable efficiency for the detection of atoms in Rydberg states, and it should be very efficient for the detection of atoms in the $2s2p^3 3s\ ^6S_{5/2}$ metastable autoionizing state. To provide an additional indication of the identity of the detected neutral atoms, the atomic beam is quenched in a dc electric field, as described below.

2.4 Quenching of Metastable Nitrogen Atoms by a Static Electric Field

Using the detection scheme just described, the metastable atomic TOF spectrum should be composed primarily of nitrogen atoms in the $2s2p^3 3s\ ^6S_{5/2}$ metastable autoionizing state and nitrogen atoms in Rydberg states. Distinction between these two types of atoms can be provided by electric field quenching as described below.

In Fig. 4, the two parallel lines labeled "charge removal region" represent a pair of parallel metal plates. A dc electric field

between these plates not only removes charged particles from the atomic beam but also shortens the lifetime of metastable atoms travelling along the flight path, because Rydberg atoms can be field ionized and the decay constants for atoms in metastable autoionizing states are expected to be field dependent. The ions and electrons produced by field ionization are removed from the beam by the electric field itself. It will be shown in the following paragraphs that the details of the quenching or suppression of the TOF spectra for the two different types of metastable atoms differ in two respects. The Rydberg atom component of the beam should be totally removed by a smaller value of applied electric field, and the time dependence of the fractional quenching observed in the TOF spectra should be qualitatively different for the two types of atoms. In practice it is necessary that use be made of both of these differences because independent observations of the quenching of the $^6S_{5/2}$ metastable state have not been made. For convenience of discussion, the time dependence of electric field quenching will be described first.

A. Time Dependence of Electric Field Quenching of Nitrogen Atoms in the $2s2p^3 3s\ ^6S_{5/2}$ Metastable Autoionizing State

A priori, for nitrogen atoms in the $2s2p^3 3s\ ^6S_{5/2}$ metastable autoionizing state, the fractional quenching is expected to depend on the time spent in the electric field as well as on the strength of the

electric field. Neglecting the effects of hyperfine structure, we expect the TOF spectra due to the natural decay of these atoms to be given by the relation

$$N(t) = N^{(0)} e^{-\gamma_o t}, \qquad (2.6)$$

where $N^{(0)}$ is the number of atoms created at t = 0 with the predestined TOF, t = L/v (see section 2.1) travelling toward the detector. Also, γ_o is the natural decay constant and N(t) is the number of atoms surviving in that state at the TOF time, t. A dc electric field of magnitude E between the two metal plates of Fig. 4 will shorten the lifetime of the metastable atoms travelling along the flight path, and the effect of the quenching field E upon the TOF spectrum of $^6S_{5/2}$ nitrogen atoms can be described as (33, 37),

$$N(t) = N^{(0)} e^{-[\gamma_o t + \gamma(E)t']}, \qquad 2.7$$

where t' is the time spent in the electric field by the travelling metastable atoms and $\gamma(E)$ is the electric field dependent decay constant. The two time intervals t and t' are related by the equation $t' = \frac{D}{L} \cdot t$, where D is the length of the electric field region.

The TOF spectra obtained for two different quench fields E_1 and E_2 are related by the ratio

$$R(t, E_2, E_1) = \frac{N(t, E_2)}{N(t, E_1)} = \frac{N^{(0)} e^{-[\gamma_o + \frac{D}{L}\gamma(E_2)]t}}{N^{(0)} e^{-[\gamma_o + \frac{D}{L}\gamma(E_1)]t}} = e^{-\frac{D}{L}[\gamma(E_2)-\gamma(E_1)]t}$$

2.8

Therefore, $$\ell n\, R(t, E_2, E_1) = -\frac{D}{L}[\gamma(E_2) - \gamma(E_1)]t\ . \qquad 2.9$$

Thus the quantity $\ell n\, R(t, E_2, E_1)$ varies linearly with time-of-flight, and the slope of the plot of $\ell n\, R(t, E_2, E_1)$ vs. t is equal to $-\frac{D}{L}[\gamma(E_2) - \gamma(E_1)]$. For $E_1 = 0$, the slope is equal to $-\frac{D}{L}\gamma(E)$. By comparing the TOF spectra for different electric fields and determining $\gamma(E)$, the functional dependence of $\gamma(E)$ upon E can therefore be obtained. It is noteworthy that although there are no experimental data near t = 0 (because of the limited range of speed of the beam atoms) any plot of $R(t, E_2, E_1)$ vs. t on a semilog paper must pass through the point R = 1 at t = 0. It will be shown in the following section that this relation, i.e., R = 1 at t = 0, is not applicable to nitrogen atoms in Rydberg states, and therefore an experimental determination of the slope of a plot of $\ell n\, R$ vs. t and its extrapolation to t = 0, can be used to differentiate between nitrogen atoms in the $^6S_{5/2}$ metastable autoionizing state and in the Rydberg states.

B. Time Dependence of Electric Field Quenching for Atoms in Rydberg Levels

The dissociative excitation process described earlier results in the production of atoms in all possible Rydberg states; therefore, a typical Rydberg atomic TOF spectrum can be described as

$$N(t) = \sum_n N_n(t)\ ,$$

where $N_n(t)$ is the TOF distribution due to atoms in Rydberg

state n, with zero external electric field. For individual nitrogen atoms in Rydberg states, the quenching in an electric field depends upon the strength of the electric field but is nearly independent of the time spent in the electric field, as is explained below.

Figure 5 shows the Coulomb potential energy, the potential energy in the external electric field, which is assumed to be applied in the -z direction, and the resultant potential energy of the Rydberg electron in an atom. It is observed that there is an extremum or maximum of the potential energy on the +z axis side of the nucleus. This maximum is hereafter referred to as the top of the barrier. Some of the unperturbed Rydberg state energy levels are also shown in the figure.

In the absence of an external electric field all Rydberg states are bound states. In the presence of an applied electric field those states whose unperturbed energy lies below the top of the barrier, decay by tunneling through the barrier. The ionization rate for these states is quite small (31, 32, 39 and Figs. 5, 6). For Rydberg states with energy greater than the energy of the top of the barrier there is no question of tunneling through the barrier, and the ionization rate is very high. In essence then, at lower electric fields the lifetime of an atom in a Rydberg state is essentially unaffected by a dc electric field until a critical electric field is reached, and then it is field-ionized very rapidly. In this picture, the average time required for field

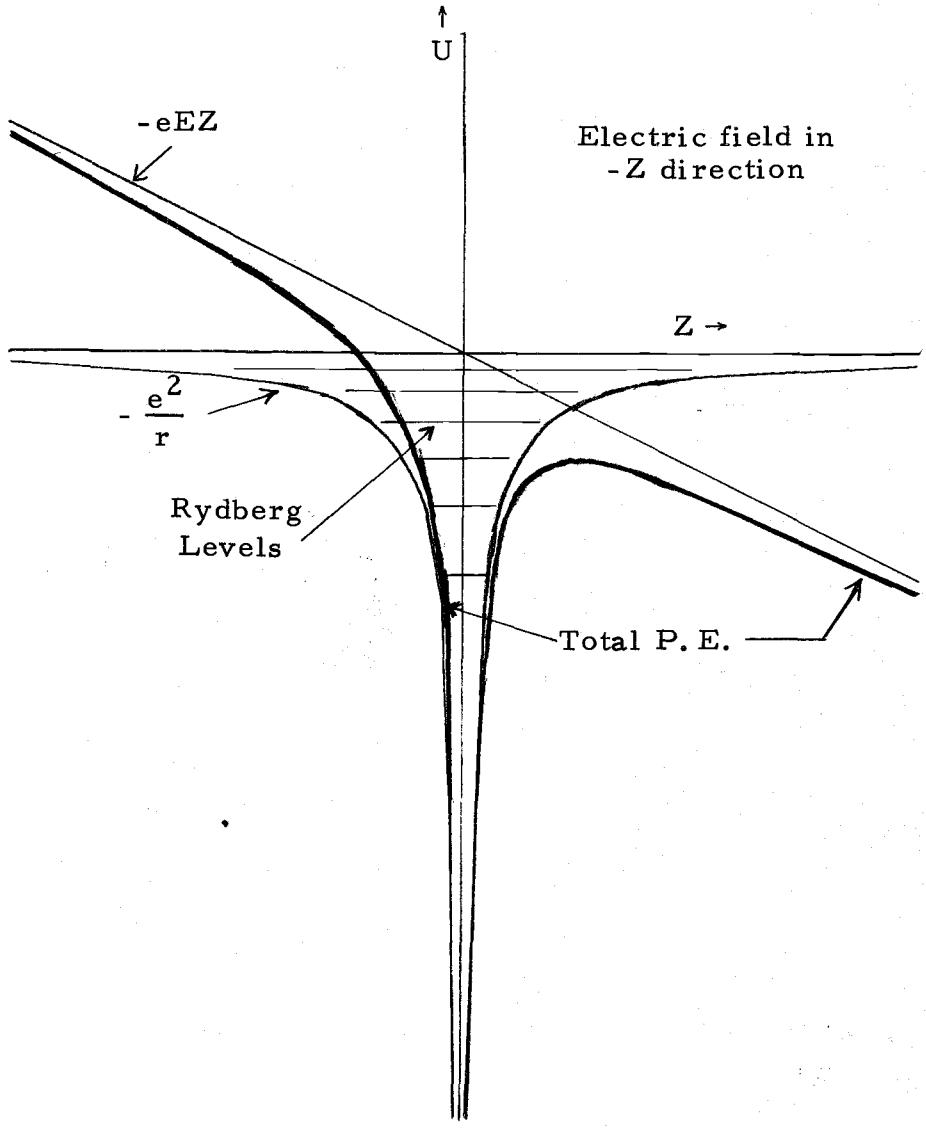

Fig. 5. Field ionization of Rydberg levels by potential modification in the presence of an external electric field.

ionization is of the same order of magnitude as the period of unperturbed motion (26), which is orders of magnitude smaller than a typical TOF for any Rydberg atom observable with the present apparatus. For example, in the Rydberg levels with n = 100, the period of a circular orbit is approximately 10^{-10} sec as compared to a typical TOF of about 10^{-5} sec. The critical electric field required for ionization of a Rydberg atom with principal quantum number n (for given ℓ) is proportional to n^{-4} (36, 38), i.e.,

$$E_c = \frac{E_o}{n^4} \qquad 2.10$$

where E_o is a proportionality constant and represents the electric field required to ionize a Rydberg atom with n = 1. It is also useful to note that for a given electric field E, there is a critical quantum number n_c, such that all Rydberg atoms with quantum number $n \geq n_c$ will be ionized. The relation between n_c and E is given by

$$n_c^4 = \frac{E_o}{E} \qquad 2.11$$

Similar results are obtained for the hydrogen atom when the problem is treated quantum mechanically (31, 32, 38) and the results are reproduced in Fig. 6. As can be seen from Fig. 6 the field ionization probability of the central component of ionized states in the n = 20 levels of hydrogen increases from 10^4 to 10^9 sec^{-1} as the strength of

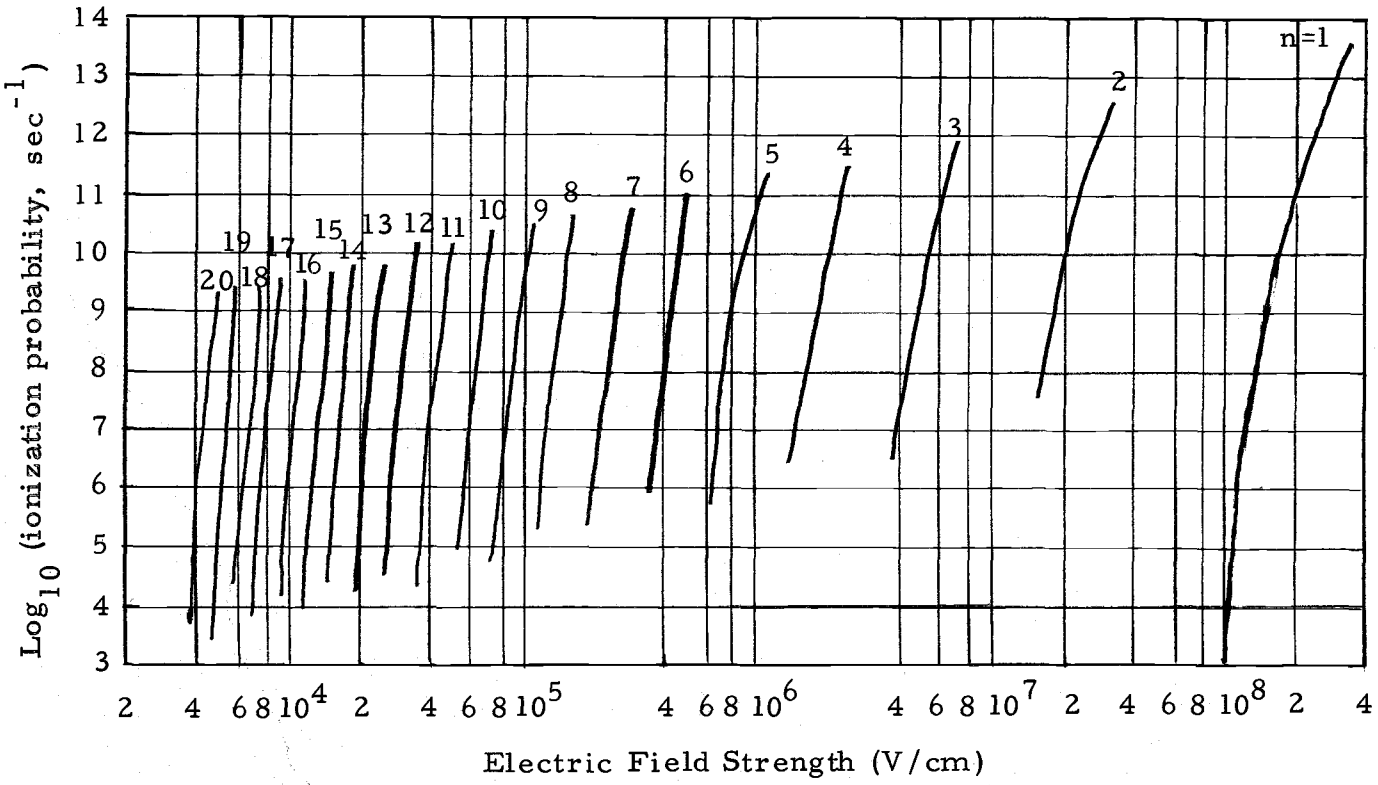

Fig. 6. Electric field ionization probabilities for the hydrogen atom for central components, defined as that with $n_1 = n_2 = (n-1)/2$ and $m = 0$ for odd n and with $n_1 = n_2 = (n-2)/2$ and $m = 1$ for even n. The relation between parabolic quantum numbers n_1, n_2 and m and the principal quantum number n is $n_1 + n_2 + |m| + 1 = n$ (43).

electric field increases from 4.0 to 5.0 kV/cm. Because the outer electron does not interact strongly with the other electrons, nitrogen atoms in Rydberg states are expected to have properties similar to those of hydrogen Rydberg state atoms.

From the above considerations, for a given electric field, all Rydberg state atoms with $n \geq n_c$ are field ionized and those with $n < n_c$ are essentially unaffected by the field. Therefore, if any TOF spectrum of metastable atoms is obtained at a given electric field, and if it is due to atoms in Rydberg states, the principal quantum number n of these atoms must be less than n_c. On the other hand, since the radiative lifetime for atoms in Rydberg states (25) is given by $\tau_n = K n^3$, where K depends upon the angular momentum of the excited states, those atoms with smaller n-value have a smaller chance of living long enough to be detected as Rydberg atoms. Thus, by using a large enough electric field it should be possible to remove essentially all of the Rydberg atoms from an atomic beam.

There is another way to distinguish between the $^6S_{5/2}$ metastable state atoms and Rydberg state atoms using a dc electric field. Even in the absence of any electric field, the TOF spectrum for Rydberg state atoms can be written as

$$N(t) = \sum_{n=n_{min}}^{n_{max}} N_n(t) = \sum_{n=n_{min}}^{n_{max}} N_n^{(0)} e^{-\gamma_{on} t} \qquad 2.12$$

where $\sum_{n}$ refers to a sum over Rydberg states, n_{min} and n_{max} refer respectively to the lower and upper limits of principal quantum numbers for which the probability of production and detection is non-negligible, and $\gamma_{on} \propto 1/n^3$.

In the presence of an electric field E, the TOF spectrum can be written as

$$N(t,E) = \sum_{n=n_{min}}^{n_c(E) < n_{max}} N_n^{(0)} e^{-\gamma_{on} t}$$

where n_c depends on E, as given by Eq. 2.11.

Similar to Eq. 2.8 for the $^6S_{5/2}$ state atoms, the TOF spectra of Rydberg state atoms for two different quench electric fields E_1 and E_2 ($E_2 > E_1$) are related by the ratio

$$R(t, E_2, E_1) = \frac{N(t, E_2)}{N(t, E_1)} = \frac{\sum_{n=n_{min}}^{n_c(E_2) < n_{max}(E_1)} N_n^{(0)} e^{-\gamma_{on} t}}{\sum_{n=n_{min}}^{n_{max}(E_1)} N_n^{(0)} e^{-\gamma_{on} t}} \qquad 2.13$$

because, all Rydberg state atoms with $n > n_c$ are quenched by the electric field irrespective of their TOF.

There appears to be no way of simplifying the relation given by Eq. 2.13, as there was in Eq. 2.8 for atoms in the $^6S_{5/2}$ state.

But it is obvious that for t = 0, $R(0, E_2, E_1) < 1$. Therefore, if $R(t, E_2, E_1)$ is plotted versus time t on a semi-log paper, and the slope of the plot is extrapolated to t = 0, the value of $R(0, E_2, E_1)$ must be different for different electric fields, and it must always be smaller than one. This is different from what is expected for the $^6S_{5/2}$ state atoms as explained earlier. Therefore, the electric field quenching can be used to distinguish atoms in the $^6S_{5/2}$ metastable state from atoms in the Rydberg states.

C. Identification using Prequench Grids

According to the discussion of the previous two sections, the electric field quenching of atoms in Rydberg states is practically independent of the length of time spent in the applied field. In contrast, the electric field quenching of atoms in the $^6S_{5/2}$ metastable state is time-dependent, as described by Eq. 2.7. Thus, it should be possible to identify the state of the beam atoms by applying an electric field confined to a very small length of flight path, and then applying a second electric field over a greater length of flight path. If the value of the electric field applied in the second quench region is always less than that in the first region, then the second field will not provide additional quenching of atoms in Rydberg states. Therefore, any additional quenching provided by the second electric field must be attributable to the quenching of atoms in the $^6S_{5/2}$ metastable state.

D. Dependence of the Quenching on the Magnitude of the Applied Electric Field

Electric field quenching was initially introduced in the present experiment because it was to be expected that the electric field needed to field-ionize essentially all beam atoms in Rydberg levels should be too small to cause significant ionization of atoms in the $^6S_{5/2}$ metastable autoionizing state. The basis for this prediction is that, since the selection rule $\Delta S = 0$ holds for both electric field ionization and Coulomb autoionization, any atom in a state which is forbidden to decay by Coulomb autoionization should not be readily ionized by a dc electric field. In addition, as is pointed out in Chapter 1, an autoionization transition usually involves a two-electron jump, whereas in the low-field limit an applied electric field can cause only transitions involving a single electron, i.e., a one-electron jump (16).

The prediction that the rate of an autoionization process should be relatively insensitive to the existence of an applied electric field has been verified in a series of experiments (1) involving the in-flight decay of beams of alkali atoms in metastable autoionizing states. With an electric field applied in essentially the same manner as shown in Fig. 4, field strengths of the order of 60 kV/cm were required to cause appreciable quenching. In contrast, in the present experiment, all detectable Rydberg atoms should be field ionized in a field of approximately 5 kV/cm.

2.5 Other Methods of Discrimination and Identification of Metastable Atoms

A measurement of the mean lifetime for natural decay can also help in the identification of the state of a metastable atom. If different from the lifetimes of known metastable states, it indicates a new state. Also, atoms in Rydberg states will show a variety of lifetimes, whereas atoms in a single metastable state must have only one lifetime.

The application of this method will be discussed in Chapter 4, where this method has been used to identify the state of the atoms.

The state of the metastable atoms in an atomic beam can also be determined by measurements which determine their Landé g-factor. A proposal for the use of these methods with a beam of nitrogen atoms will be discussed briefly in Chapter 6.

3. EXPERIMENTAL SETUP

A schematic cross-sectional view of the time-of-flight apparatus used in the present experiment in shown in Fig. 7. The details of the excitation chamber, electron gun, detector and electronics used in the experiment will now be discussed.

By comparison with known decay rates of atoms in metastable autoionizing states (1-4), nitrogen atoms in the $2s2p^3 3s\ ^6S_{5/2}$ metastable autoionizing state are expected to have a natural lifetime larger than 10^{-6} sec. Since nitrogen dissociation fragments are expected to have speeds of the order of 10^6 cm/sec, a relatively short TOF apparatus may be required. In the present apparatus the TOF path length is 15.3 cm. In order to avoid collisional quenching along a path of this length the operating pressure should be less than approximately 10^{-4} Torr. To avoid contamination of the TOF spectra by metastable atoms produced by dissociative excitation of the molecules of the background gas, a much lower base pressure is needed.

3.1 Excitation Chamber and Vacuum System

The excitation chamber and atomic beam flight path consists of a two-liter cylindrical stainless-steel chamber which is pumped to a base pressure of about 10^{-7} Torr with a two inch stainless steel oil diffusion pump (Consolidated Vacuum Corporation) and a pellet-type

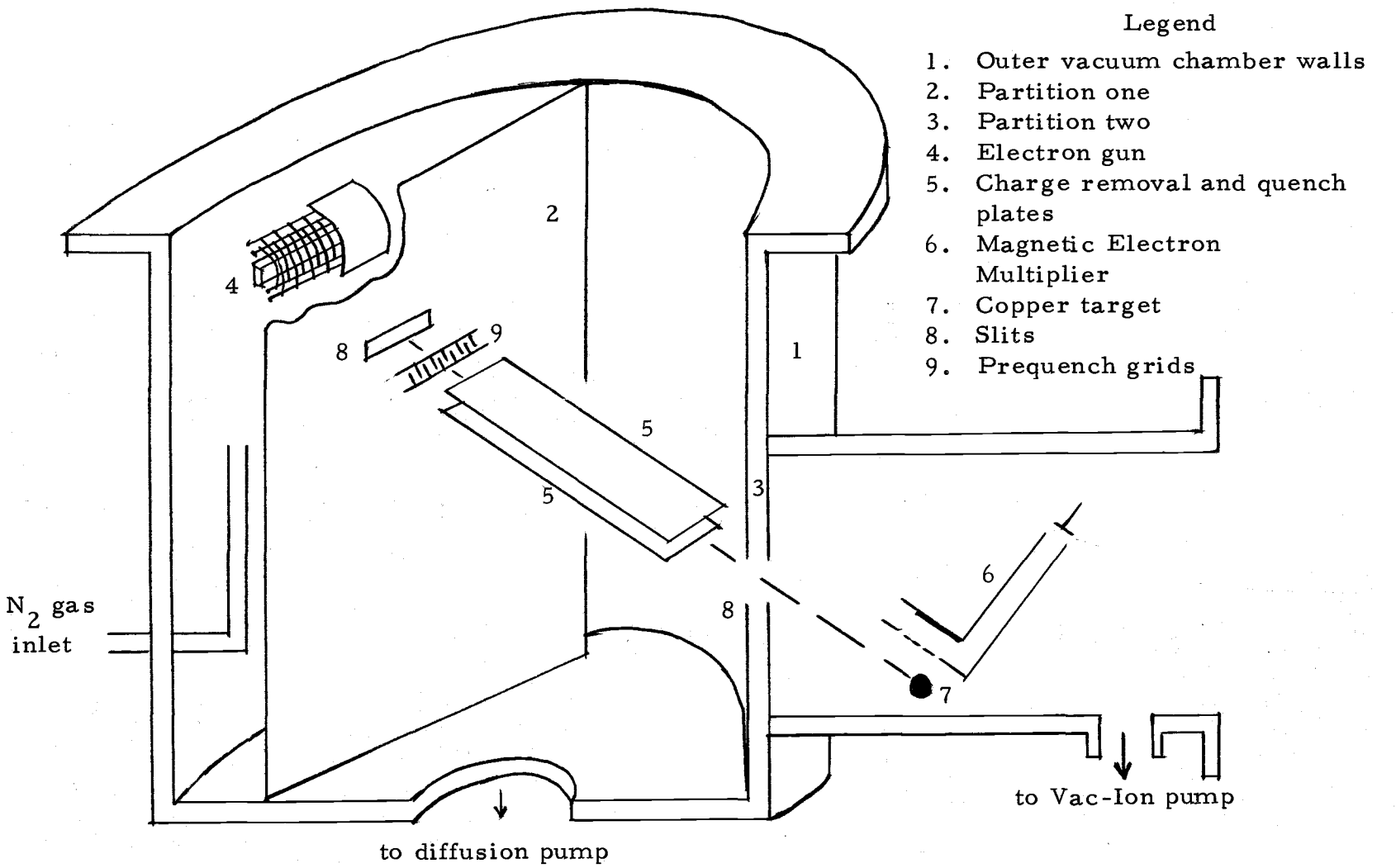

Fig. 7. Schematic cross-sectional view of the vacuum system.

trap filled with Sorbent A (Trademark CVC), which serves as an oil absorber between the pumping system and the excitation chamber. During pumpdown, the Sorbent A pellets are baked at a pressure of approximately 10^{-2} Torr to drive off absorbed water vapor. Therefore, the Sorbent A is changed at each opening of the vacuum system to prevent contamination of the excitation chamber and electron gun by pump oils during the following bakeout. A pneumatic gate valve is fixed between the diffusion pump and the vacuum chamber. This valve is closed automatically during an electrical power failure to prevent damage to the excitation chamber by pump oils. Furthermore, it is closed during the initial starting period of the diffusion pump to prevent backstreaming of diffusion pump oil into the excitation chamber. A liquid nitrogen trap is placed between the forepump and the diffusion pump, and the combined effect of it and the pellet trap is to reduce the base pressure from about 10^{-6} to 10^{-7} Torr. To minimize the effect of background gases, it is necessary to evacuate the system to such low pressures before the experimental gas is introduced.

The main vacuum chamber is divided by two partitions into three sections as shown in Fig. 7. In one section there is a gas inlet system and an electron gun, and, as is indicated in Fig. 7, the nitrogen gas enters the electron gun nearly perpendicular to the flight path. The second section contains two parallel stainless steel plates. These plates are rectangular with a width of 3 cm and a length of 6 cm.

The plates are connected to dc power supplies to produce an electric field perpendicular to the atomic beam flight path. The field serves the dual purpose of removing charged particles from the beam and providing identification of neutral particles, as discussed in the preceding chapter. The first and second sections of the vacuum system are connected by a rectangular slit of dimensions 0.2 cm by 1.0 cm.

The third section of the main vacuum system is a 1-liter cylindrical stainless steel chamber welded to the 2-liter chamber. In Fig. 7 this section of the apparatus is shown in cross section rather than in perspective. It is pumped by an 8-liter/sec (Varian Associates) Vac-Ion pump, and is connected to the charge removal and quench plate region by a slit which is identical to the one described above. In this way a pressure differential is maintained between the electron gun and the detector regions during an experiment. The pressure of N_2 target gas at the electron gun can be varied from 5×10^{-6} to 4×10^{-4} Torr, while the pressure at the detector is usually at least a factor of ten lower than that at the electron gun.

3.2 Prequench Grids

The prequench device consists of a series of 40 parallel wires, intersecting the flight path perpendicularly and oriented perpendicular to the beam axis. Alternate wires of the grid device are biased at a common potential. Small wires are used in order to minimize surface

effects. The center to center spacing between adjacent wires of different grids is 0.5 mm and the diameter of each wire is 0.1 mm. The device is shown below in Fig. 8.

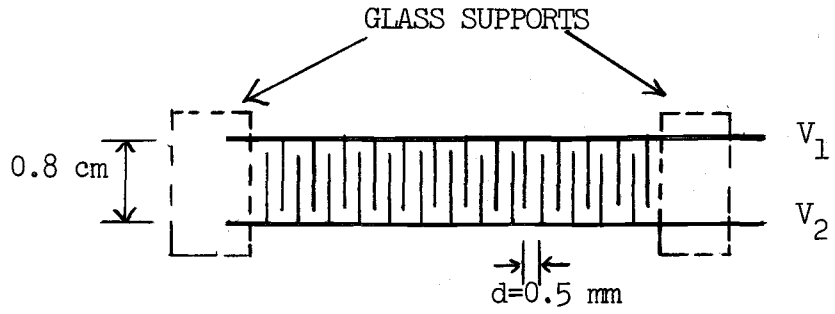

Fig. 8. Diagram of prequench grids.

For a potential difference V between the adjacent wires separated by a distance d and each of radius a, the electric field at a point in the plane of the wires and at a distance r from one of the wires is given by

$$E = \frac{V}{2 \ln(\frac{d-a}{a})} (\frac{1}{r} + \frac{1}{d-r}) \qquad 3.1$$

The electric field, in the plane of the wires is minimum at a point midway between the wires, i.e., at $r = d/2$, and maximum at a point on the surface of the wires, i.e., at $r = a$. Therefore,

$$E_{min} = \frac{2\,V}{d\,\ln(\frac{d-a}{a})} \qquad 3.2$$

and

$$E_{max} = \frac{V}{2\,\ln(\frac{d-a}{a})}\,(\frac{1}{a} + \frac{1}{d-a}) \qquad 3.3$$

For the prequench grid used in the present experiment, a = 0.05 mm, d = 0.5 mm, therefore,

$$E_{min} = 18.2\ V \text{ volts/cm} \qquad 3.4$$

and

$$E_{max} = 50.57\ V \text{ volts/cm} \qquad 3.5$$

where V is the potential difference in volts between the adjacent wires.

3.3 Gas Handling and Pressure Measurement

A steady flow of nitrogen gas through the vacuum system is maintained by a standard gas handling system. Nitrogen gas of 99.99% purity is used and is let in through a Matheson Model 18 ultrapure pressure regulator (with an advertised inboard leak rate less than 8×10^{-10} cm^3/sec) followed by a fine control needle valve (Vacuum Accessories Corporation of America).

The gas pressures are measured with Varian Associates nude

ionization gauges and a dual-range power supply, Model 971-0014. In the first section, containing the electron gun, the pressure is measured with a high-range nude gauge (pressure range 10^{-1} to 10^{-6} Torr). In the second section a low-range nude gauge (pressure range 10^{-5} to 10^{-11} Torr) is employed. Since both gauges are mounted inside the vacuum system, they are turned off during the actual experiment, so that the radiations, ions and electrons produced in the gauges while they are on, do not contaminate the TOF spectra. In the third section, containing the detector, the pressure is measured by the Vac-Ion pump power supply.

3.4 Electron Gun

In order to obtain high resolution TOF spectra, the dimension of the excitation region parallel to the atomic beam flight path should be much smaller than the 15.3 cm length of the flight path. A very good high-resolution geometry is available in the RCA 6AH6 receiving tube. This tube has a 1 mm by 2 mm cathode of rectangular cross section, and a length of 15 mm. Both the control grid and the screen grid are also of essentially rectangular geometry, and the cathode-to-grid and grid-to-grid separations are only 0.35 mm. The approximately rectangular shape of the electron gun cathode and grid structure provides a similarly shaped atomic beam source. A perspective view and an end on view of these essential parts of the 6AH6 tube are shown

in Fig. 9, and a cross-sectional view of the tube, in its optimum geometry, is shown in Fig. 7. With both grids grounded and the cathode pulsed negatively, an excitation region of less than 1 mm in length, in the direction of the atomic beam flight path, is provided. Also, a magnetic field of 10 to 100 gauss, produced at the electron gun by the two Helmholtz coils (Fig. 4) placed outside the vacuum system, provides additional confinement of the excitation region.

Before the electron gun is mounted in the vacuum system, the glass jacket of the 6AH6 tube is cut around the tube base (near the mica sheet of the tube) and then the top part of the glass tube is removed. The tube plate, i.e., the anode, is then removed, and the remainder of the tube assembly, shown in Fig. 9, is used as the electron gun. The electron gun is placed in the vacuum system as soon as possible after removing it from the glass jacket, to minimize deterioration of its oxide-coated cathode. The vacuum system is evacuated to 10^{-6} Torr with the electron-gun filament at 0.5 volts. The gun is then activated slowly as the filament voltage is increased to 6.4 volts by which time the cathode material is almost completely outgassed. Though the gun filament is rated for 6.4 volts, generally the filament voltage is maintained between nine and twelve volts to obtain a high emission of electrons. The filament voltage is supplied by a dc regulated voltage power supply with one terminal grounded.

The electron gun is pulsed by applying a negative voltage pulse

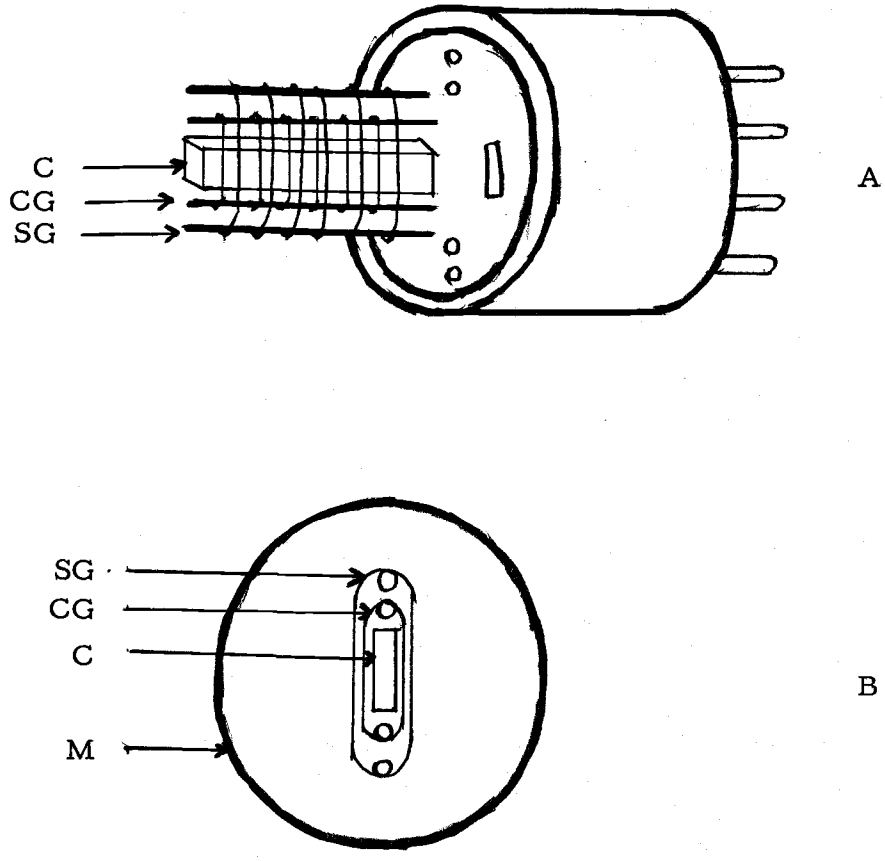

C -- Cathode

CG -- Control grid

SG -- Screen grid

M -- Mica disc

Fig. 9. Diagram of electron gun (part of 6AH6 tube) used in the experiment. A - side view, B - cross-sectional view.

to the cathode, with all grids at electrical ground or biased a slightly negative voltage. A slight negative voltage on grids keeps the electrons confined near the cathode during the dead time following the excitation pulse, thus reducing the background noise at the detector.

A pulse generator, E-H Model 132-A is used to provide negative rectangular voltage pulses, variable in both height and width. Pulse heights from 30 to 160 volts and widths from 0.4 to 2.0 μsec are used in the present experiment. The pulse generator is specified by the manufacturer to have a maximum pulse height of 50 volts when it is terminated by a 50 Ω resistor. Pulse heights as large as 160 volts can be obtained by terminating the output of the pulse generator in a 450 Ω resistor.

3.5 Timing Electronics

Electronic instruments are used to measure the time-of-flight. When the pulse generator gives a negative pulse to the cathode of the electron gun, the electrons bombard N_2 molecules, and excitation and dissociation takes place. The pulse generator also produces a trigger pulse which starts the charging ramp of a time-to-pulse-height converter (Ortec Model 437A). The TPHC ramp is stopped by a pulse from the detector. If the stop pulse is initiated by a particle originally produced or excited by the electron gun pulse, then the particle's TOF is proportional to the amplitude of the corresponding output pulse from

the TPHC. Output pulses from the TPHC are stored in a pulse-height-analyzer (Technical Measurement Corporation, Model 404), and a TOF spectrum is accumulated by regular repetition of the electron-gun pulses. As was noted in Chapter 2, it is important that, in order for this spectrum to represent the velocity distribution of particles produced at the electron gun, the total count rate must be so low that the probability for the occurrence of two or more detector pulses during one cycle of operation is negligible. The electron-gun pulse repetition rate is typically 2000 sec^{-1} and the total count rate is always less than 200 sec^{-1}. In the present experiment, slow metastable N_2 molecules require approximately 0.5 msec to reach the detector and therefore determine the maximum repetition rate. Since the count rate is less than 200 sec^{-1}, there is negligible "pile up" in the system, i.e., there is a negligible probability that an input of one pulse will be received by any component while another pulse is still being processed. Since the pulse-height analyzer can process approximately 10^4 pulses per second and the count rate is always much less than this value, there is negligible pile up in this component of the electronics.

The detector output pulse is first preamplified by an Ortec Model 109 A preamplifier and then by an Ortec Model 410 linear amplifier. The output of the linear amplifier is connected to the stop-input of the TPHC.

The electron-gun input pulse couples inductively as a low-level

signal in the output of the preamplifier, which serves as an excellent timing event for checking delays and timing sequences. A Tektronix Model 545B oscilloscope is used to display the output pulses from the amplifier, and a Baird-Atomic Inc. Abacus Model 124 scaler is used to monitor the count rate.

The TOF spectrum from the pulse-height-analyzer is printed on a TMC Model 500 printer and reproduced on a Hewlett Packard Model 7004B X-Y recorder.

3.6 External Magnetic Field Coils

A pair of magnetic field coils, each coil having 500 turns and a mean radius of 11 cm, is mounted outside the vacuum system. Whereas the original purpose of the magnetic field was to confine the electrons to the excitation region, it also serves to remove ions produced in the electron gun by deflecting them. This is particularly important when the TOF spectra are taken at low values of the electric field between the quench plates.

A coil current of as high as 3 amperes, with iron slugs within the coils, is capable of producing a magnetic field of 20 gauss in the region of the electron gun.

3.7 Detector

Referring to Fig. 7, the third section of the vacuum system

contains the detection system. The detection system consists of a copper target and a magnetic electron multiplier (MEM).

The copper target is a short piece of No. 12 copper wire placed in the flight path of the neutral particles defined by the two slits. In this way, the copper target serves to effectively terminate the flight path of the photons, neutral atoms and molecules which come from the beam source. Photons are mostly absorbed by the target, but some are reflected in different directions. Those reflected into the MEM are the ones detected and recorded in the PHA. Both photons and metastables (atoms and molecules) can eject Auger electrons from the target, but these electrons cannot enter the MEM because it is biased negatively with respect to the Cu-target. As has been discussed in Chapter 2, nitrogen atoms in Rydberg levels or in the $^6S_{5/2}$ metastable autoionizing state should be ionized at or near the copper target, and the resultant ions are accelerated toward the cathode of the MEM. These energetic ions (K.E. $\simeq$ 1 KeV) produce secondary electrons at the MEM cathode, which are then multiplied to form the output pulses.

For several sets of data, the copper target was replaced by a stainless-steel plate. No observable effect on either the TOF spectra or the electric-field quenching effect was found. Both positive and negative voltages on the copper target were tried. For voltages on the copper target more negative than those on the MEM, no atomic

TOF spectra were obtained. This is confirmation that positive ions are being detected by the MEM, and that only the metastable atoms which undergo surface ionization are detected.

The MEM is arranged almost perpendicularly to the flight path and hidden from the beam of metastable particles, so that only the reflected photons or positive ions created at the copper target can enter it. The description and functioning of the MEM is given below.

The cross-sectional view of magnetic electron multiplier (Bendix Model M308), labeled MEM in Fig. 4, is given schematically in Fig. 10. It consists of two high-resistance strips. It has a tungsten plate for the cathode. The MEM has no activated surfaces and thus can be removed from the vacuum system without damage to the cathode and dynode structure. It consists of a 90% optically transparent metallic entrance grid, a tungsten cathode, a coated glass dynode strip, a coated glass field strip and a stainless steel anode plate. The dynode and field strips are coated with high resistance material, and each measures about 100 Megohms along its 4.5-cm length. They are mounted parallel to each other with a separation of 0.25 cm inside a small permanent magnetic structure which produces a uniform magnetic field of about 400 to 600 gauss perpendicular to the plane of Fig. 10. The thin solid lines indicate conductors, and the numbers give the voltages applied to the MEM.

When photons or positive ions enter MEM, they eject electrons

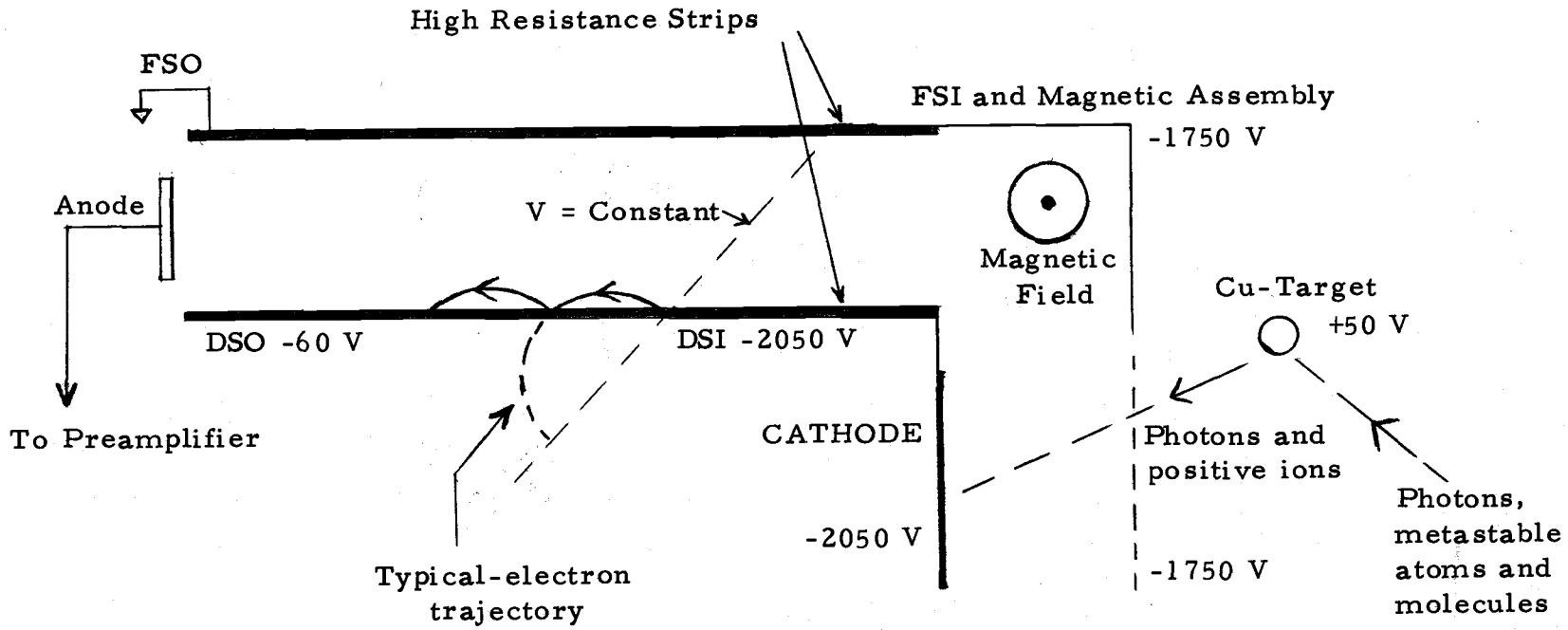

Fig. 10. Schematic diagram of the detection system, copper-target and Magnetic Electron Multiplier.

from the cathode with essentially zero velocity. These electrons find themselves in crossed electric and magnetic fields. The path for each electron is a cycloid whose cusps fall along an equipotential line as shown in Fig. 10. The number of electrons increases at each cusp, and at the anode each pulse contains about 10^6 electrons. Thus for each photon or positive ion entering the MEM there will be an electron (or negative) pulse output from the anode. The average time required for the pulse to travel inside the MEM is of the order of 10^{-8} sec (30, p. 29), which is much smaller than the TOF of the atoms. The bias voltages on the MEM are adjusted to yield a maximum count rate for metastable atoms. It should also be mentioned that as far as photon detection is concerned, the MEM is most efficient in the extreme ultraviolet range, particularly in the range 200-1400 Å. This feature of the MEM is particularly important and will be discussed in Chapter 4.

4. EXPERIMENTAL RESULTS AND DISCUSSION

4.1 TOF Spectra at Different Electron Gun Pulse Heights

For a flight path of 15.3 cm, the TOF spectra obtained for three different electron gun pulse heights are shown in Fig. 11. The zero of the time of these spectra was determined from the position of the fluorescence photon peak, which is present at all electron gun pulse heights greater than approximately 10 volts. The width of the photon peak corresponds closely to that of the electron gun pulse. The fluorescence photon peak is followed by a small contribution due to afterglow. These are not shown in the TOF spectra of Fig. 11. Also not shown is a very small and "fast peak" which occurs at approximately channel 14 (5.6 μsec) and is present for electron gun pulse heights greater than 70 volts. This fast peak could possibly be due to neutral atoms or molecules produced by charge exchange of fast ions in the excitation region.

The TOF spectra are obtained by adjusting various parameters for most optimum conditions. For example, keeping the filament current at more than 550 mA results in an increased afterglow after the photon peak and, consequently, a higher value of background counts in the "valley" before the metastable atomic TOF spectra. Also, for large filament currents, the background noise was large. Generally the electron gun is energized by pulsing the cathode negatively and

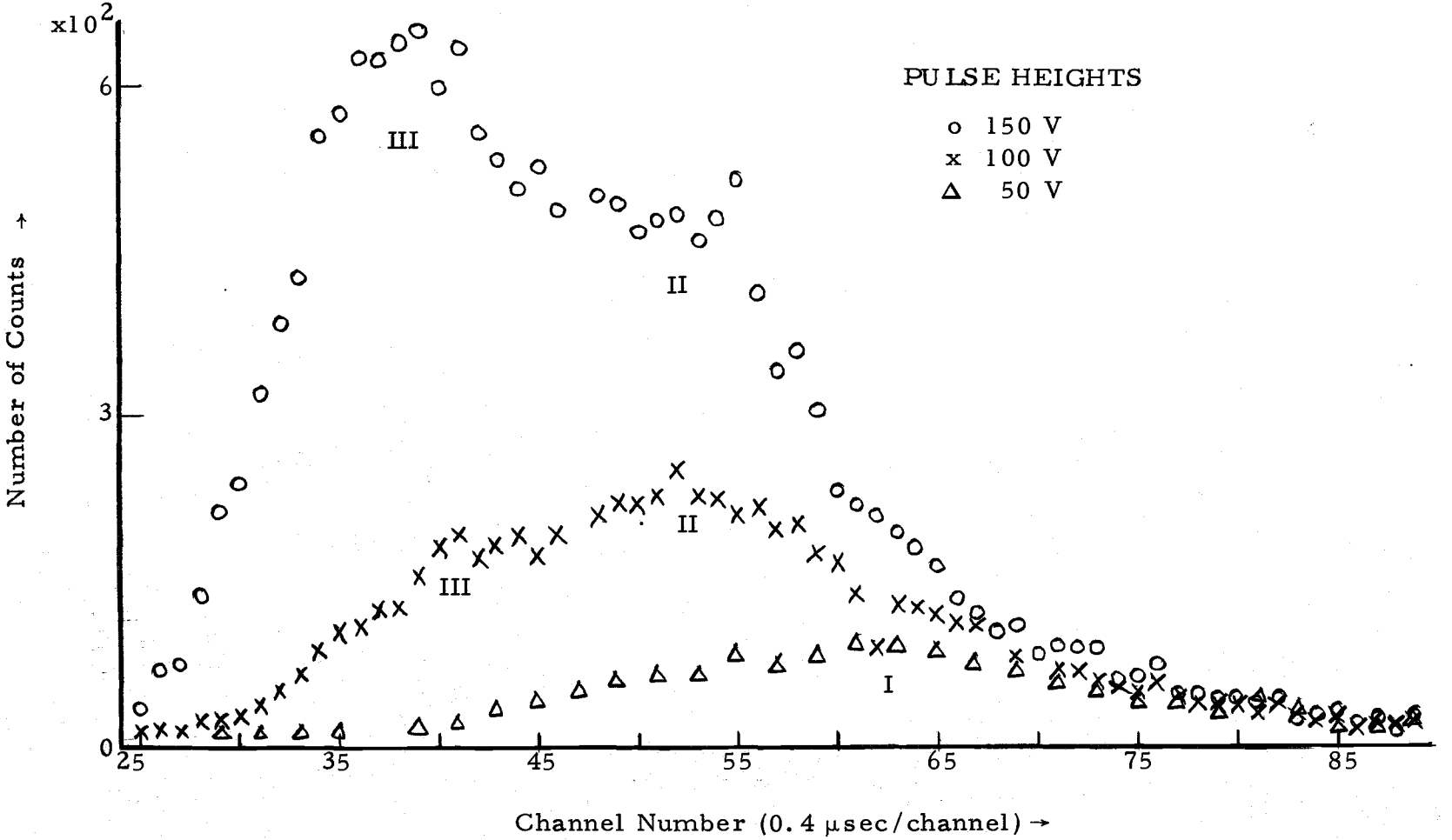

Fig. 11. TOF spectra at different electron gun pulse heights. The TOF spectra for 150 V and 100 V pulse heights were accumulated for 10 min each; TOF spectrum for 50 V pulse height was accumulated for 20 min and with increased pulse width. Each channel represents 0.4 μsec. The pressure of N_2 gas in the source region was 4×10^{-5} Torr.

either grounding the grids or biasing them at a small negative voltage. If, instead the cathode is grounded and the grids are pulsed positively, the afterglow increases to the extent that the atomic TOF spectra are significantly contaminated. It was also found necessary to bias both of the charge removal, or quench plates negatively, at approximately 200 V, so as to minimize the afterglow and background noise. The pressure of N_2 gas in the excitation region is generally of the order of 5×10^{-5} Torr. With the increase of pressure, the overall and metastable atomic count rate increases practically linearly with the pressure. No effect on the position of TOF spectra or any distortion in shape is observed even at a pressure of 10^{-4} Torr.

By comparison with Fig. 3, it is obvious that the TOF spectra of Fig. 11, are due to metastable nitrogen atoms and not due to photons, ions and molecules. For the TOF spectra of Fig. 11, the kinetic energy range is approximately from 10 eV to 2.5 eV. For metastable atoms produced by dissociative excitation, it is not unusual that the fragment atoms have kinetic energies in this range (See Fig. 2). As is mentioned in Chapter 2, since the detection scheme used in the present experiment is not capable of detecting to an appreciable extent atoms in the ^4S ground state and ^2D and ^2P metastable states, the TOF spectra of Fig. 11, cannot be due to atoms in these states. This conclusion is further confirmed by the observation of electric field quenching and lifetime measurement, which will be discussed

later in this chapter. Therefore, the TOF spectra of Fig. 11 could possibly be due to nitrogen atoms either in the $^6S_{5/2}$ metastable state or in Rydberg states. Further identification of the state of these atoms is achieved principally by the electric field quenching results and is discussed in the following three sections.

All of the electron gun pulse heights used for the data shown in Fig. 11, are large enough that many different dissociative molecular potential curves (See Fig. 2 and its discussion) can be important in the production of these spectra; therefore, the spectra by themselves do not serve to identify the detected atoms. It is also not possible to explain in detail the different prominent features (labeled I, II and III in Fig. 11) of these spectra. For identification of atoms by electric field quenching, the largest possible range of TOF is required, therefore, electron gun pulse heights of approximately 150 V are usually used for the electric field quenching measurements.

4.2 TOF Spectra at Different Electric Fields

The TOF spectra for six different electric fields and for 140 V effective electron gun pulse height, are shown in Fig. 12. These TOF spectra obtained for different electric fields, were accumulated for the same length of time, 160 minutes, by storing data at each value of applied electric field in intervals of 10 min each and in cycles of first increasing electric field and then decreasing electric field, and

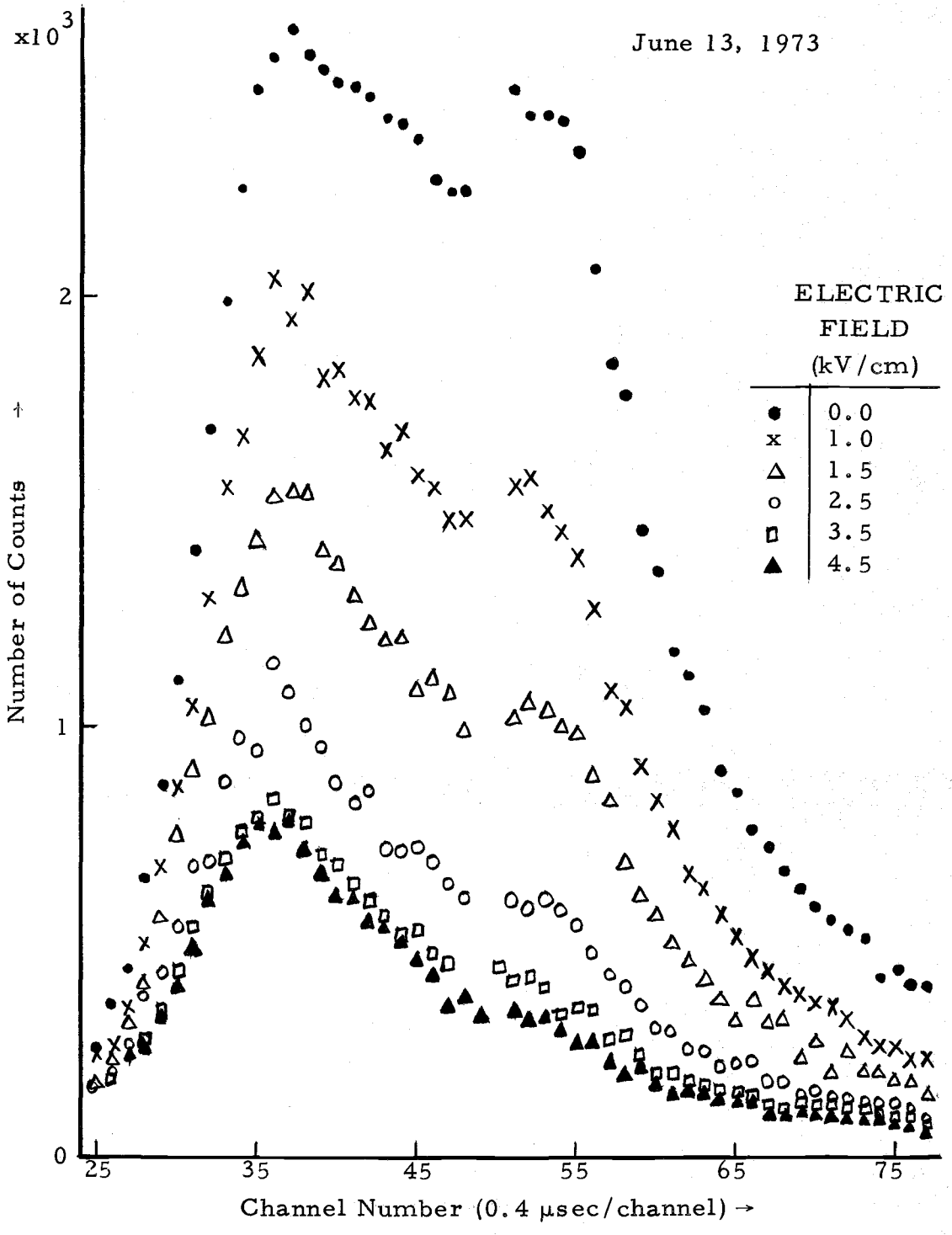

Fig. 12. TOF spectra at different quenching electric fields. Electron-gun pulse height = 140 V, width = 0.38 μsec, rep. rate = 20 kHz, N_2 pressure = 4×10^{-5} Torr, and channel width = 0.4 μsec. Channel number 1 corresponds to the beginning of the excitation.

then repeating the cycles. This procedure was adopted to minimize the effects of pressure variation and fluctuations in the electron-gun filament current. The specifications of various other parameters related to the TOF spectra of Fig. 12 are given in Table II.

It is noteworthy that with the change of the electric field between the quench plates, the number of photons accumulated in the photon peak did not vary more than 5%, and only those data were considered for interpretation for which the number of photons in the TOF spectra of different electric fields were nearly equal. In addition to the same time of accumulation of TOF spectra for different electric fields, an equal number of photons also provide a basis for normalization, and also confirms that the efficiency of electron gun is not affected by the electric field.

It is to be observed in Fig. 12, that for the TOF spectra at electric fields of 3.5 kV/cm and 4.5 kV/cm, there does not appear to be much additional quenching in earlier channels, approximately from channels 25 to 35. This is possibly due to the fact that N_2^+ ions which are created copiously in the electron gun during excitation, are accelerated by the quench plates which are biased negatively. When these ions smash into the plates, they eject electrons which can cause all of the excitation reactions to occur (See Section 2.1). The TOF spectra due to the metastable atoms created in the quench region will superimpose over the TOF spectra of metastable atoms created

Table II. Specifications of the experimental conditions for the TOF spectra of Fig. 12.

1. Length of flight path = 15.3 cm

2. Length of quench plates along the flight path = 6.0 cm
   Distance between the quench plates = 1.0 cm

3. Base pressure = 2×10^{-7} Torr
   Pressure with N_2 gas in excitation region = 4×10^{-5} Torr

4. Electron gun: Filament current = 550 mA Voltage of grids = -10
   Pulse height = -150 V Pulse width = 0.38 μsec
   Pulse rep. rate = 20 kHz
   Effective pulse height = -140 V

5. Detector voltages: DSO = -60 V DSI = -2050 V
   FSO = 0.0 V FSI = -1750 V
   Magnetic assembly = -1750 V
   Cu target = +50 V

6. Voltages of prequench grids: $V_1 = V_2 = 0$

7. TPHC span = 40 μsec
   Corresponding number of channels on PHA = 100

8. Current in the Helmholtz magnetic field coils = 3 amperes, and small permanent magnets are used.

9. Voltages on quench plates: Voltage on lower plate = -0.5 kV
   Voltages on upper plate = -0.5, -1.5, -2.0, -3.0, -4.0, -5.0 kV
   to give electric fields of: 0.0, 1.0, 1.5, 2.5, 3.5 and 4.5 kV/cm respectively.

10. Average number of counts per sec (including photon counts) = 80

11. Total accumulation time for each electric field = 160 min

12. Total number of metastagle atom counts (from channel 25 to 74)
    a. at E = 0 kV/cm $\cong$ 76000
    b. at E = 4.5 kV/cm $\cong$ 15000

13. Total number of photons in channel one $\cong$ 185000

in the electron gun. Since, for the metastables created in the quench region, the flight path is shorter, they will contaminate only the earlier part of the TOF spectra. As is obvious from Fig. 12, this effect increases with the increase of electric field, and it is for this reason that TOF spectra at higher electric fields were not accumulated. The contamination could probably be avoided by replacing the quench plates with metallic screens; however, this was not done because the contamination effect does not alter the conclusions of the present experiment.

Approximately 100 sets of data similar to those of Fig. 12 have been obtained, under different sets of experimental conditions, using different pulse heights, different pressures, different combinations of voltages on the quench plates etc. Some of these data have been published earlier (33), and all are very similar to those of Fig. 12.

From Fig. 12, it is observed that even with an applied electric field of 4.5 kV/cm, the TOF spectra due to metastable atoms are not wholly quenched. If the TOF spectra are due to nitrogen atoms in the Rydberg states, then at a field of 4.5 kV/cm, all Rydberg-state atoms with principal quantum number $n \geq 22$ must be quenched (32). For Rydberg-state atoms with $n < 22$, in p-levels, the lifetime is less than 2 μsec (25, 26). Since the TOF for these atoms varies from 10 to 40 μsec, each Rydberg atom with $n < 22$ has a very small probability of reaching the detector in the state in which it is created in the

source. For example, for Rydberg atoms in the 22p levels,

$$N_{22}(t) = N_{22}^{(o)} e^{-t/2.1} \qquad 4.1$$

where t is the TOF, measured in microseconds, N(t) and $N^{(o)}$ have the same meaning as in Chapter 2, and the subscripts refer to the atomic 22p levels. Using the average TOF, 25 μsec, yields

$$N_{22}(25) = N_{22}^{(o)} e^{-25/2.1} , \qquad 4.2$$

or

$$\frac{N_{22}(25)}{N_{22}^{(o)}} \simeq e^{12} \simeq 10^{-5} . \qquad 4.3$$

It will now be shown that the occurrence of such a large decay factor for the detected atoms is inconsistent with the observed photon count rate.

The photons which reach the detector are produced predominantly at the electron gun during the excitation pulse. They of course do not decay in flight, and their TOF is essentially zero. Therefore,

$$N_\gamma(t) = N_\gamma^{(o)} = N_\gamma ,$$

where γ refers to photons. If the entire atomic TOF spectrum for an applied electric field of 4.5 kV/cm is assumed to be located at the average TOF (≃25 μsec), then, from the experimental data of Fig. 12 and Table II,

$$\frac{\varepsilon_{\gamma} N_{\gamma}}{\varepsilon_{22} N_{22}^{(25)}} \cong 10 \ , \qquad 4.4$$

where ε_{γ} and ε_{22} refer to the overall detection efficiencies for photons and Rydberg-state atoms respectively. Since the detector is designed to detect positive ions and it is "hidden" from photons, as is discussed in detail in Chapter 3, it is reasonable to assume that the efficiency for the detection of Rydberg-state atoms (or atoms in the $^6S_{5/2}$ metastable state) is larger by a factor of 10^3 to 10^5 than the detector efficiency for photons, i.e.,

$$10^3 \varepsilon_{\gamma} \leq \varepsilon_{22} \leq 10^5 \varepsilon_{\gamma} \qquad 4.5$$

For the sake of illustration, it is assumed that $\varepsilon_{22} = 10^4 \varepsilon_{\gamma}$, therefore, from Eq. 4.4,

$$\frac{N_{\gamma}}{N_{22}^{(25)}} \cong 10^5 \qquad 4.6$$

and, from equations 4.3 and 4.6,

$$\frac{N_{\gamma}}{N_{22}^{(o)}} \cong 1 \ .$$

In contrast to this illustration, it is to be expected that if the observed TOF spectra represent atoms in Rydberg levels, N_{γ} should be several orders of magnitude larger than $N_{22}^{(o)}$, as is explained below.

It is well known that most of the extreme ultraviolet light emitted by atomic and molecular nitrogen arises from resonance transitions, i.e., transitions between low lying levels in the ground state configuration and low lying excited levels. For example, the strongest emission lines in atomic nitrogen arise from the transitions

$$2p^2 3s\ ^4P \rightarrow 2p^3\ ^4S\ ,$$

and these transitions lie at a wavelength of approximately 1200 Å. Also, because of the effects of wave function overlap, it is expected that the cross-sections for the excitation of low lying excited levels should be much larger than the cross sections for dissociative excitation to atoms in Rydberg levels. Finally, for almost all cases of dissociative excitation to atoms in Rydberg levels, dissociative ionization is a strongly competing process (22).

By combining these three effects, it is possible to predict that $N_\gamma >> N_{22}^{(o)}$, in contrast to the results of the above illustration. Since the illustration is quite representative of experimental data, it is reasonable to conclude that the TOF spectra obtained when the beam of atoms passes through a strong dc electric field are not due to atoms in Rydberg levels. In contrast, according to the discussion of Chapter 1, the natural lifetime of $^6S_{5/2}$ metastable state of nitrogen may be as large as 10^{-4} sec, and beam atoms in this state should not be severely quenched in the electric fields used here (1, 37).

Therefore, for the purpose of the present discussion, the decay of atoms in the $^6S_{5/2}$ metastable state along the beam path may be neglected, and the ratio of photons produced to metastable atoms produced is predicted to be of the order of 10^5. It is noteworthy that the lifetimes of nitrogen atoms in the metastable ^2D and ^2P levels should be essentially uneffected by an electric field of 5 kV/cm, therefore, the observed electric field quenching confirms the previous conclusion that the detected metastable atoms are not in the ^2D and ^2P low lying metastable states.

4.3 Identification Based on TOF Spectra Obtained with the Prequench Electric Field

Figure 13 shows two TOF spectra obtained with a 100 V potential difference between the adjacent wires of the prequench grids (Fig. 8). For this potential difference, there is a minimum electric field of 1.8 kV/cm at the mid-point between the adjacent grid wires and in the plane of the grid wires (See Section 3.2). The electric field between the quench plates for the upper and lower TOF spectra are 0.3 kV/cm and 1.5 kV/cm respectively; thus, for both spectra the electric field between the quench plates is smaller than the minimum electric field in the prequench grid region. It is obvious that the two TOF spectra shown in Fig. 13 are not identical, and that the increase in the electric field between the quench plates causes additional quenching of the beam

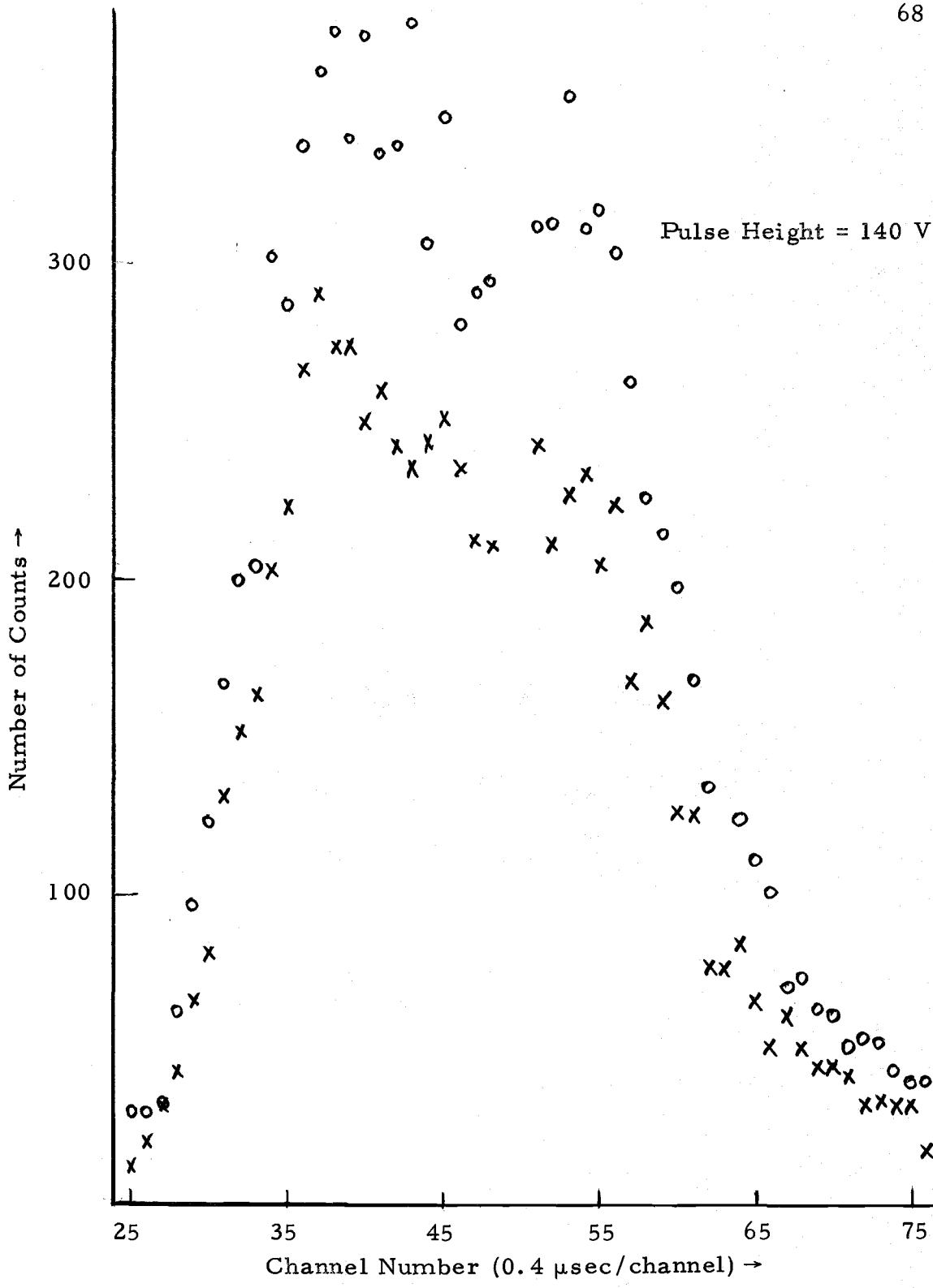

Fig. 13. TOF spectra with prequench-grid electric field. For both TOF spectra, grid voltages: $V_1 = -100$ V, $V_2 = -200$ V, $\Delta V = 100$ V which gives $E_{min} = 1.8$ kV/cm in the prequench region. The electric field between quench plates for circles and crosses is 0.3 kV/cm and 1.5 kV/cm respectively.

atoms. Therefore, according to the discussion of Section 2.4C, the difference of the two spectra must represent only atoms in the $^6S_{5/2}$ metastable state.

The prequench device was introduced in the experiment essentially to prequench the Rydberg-state atoms and to get TOF spectra of atoms in the $^6S_{5/2}$ state. Unfortunately its importance was not fully understood at the time the experiment was done. Specifically, its use in conjunction with the quench plate field to provide identification of beam atoms was not fully appreciated. Thus the data presented in Fig. 12 are the only data where the TOF spectra are obtained for values of electric field between the quench plates smaller than the minimum value of the electric field in the prequench region. However, there are several sets of data where, for the second TOF spectrum, the value of the electric field between the quench plates is only slightly higher than the minimum value of the electric field in the prequench region. All of these data are similar to those presented in Fig. 13 and they provide qualitative support to the conclusion derived above.

In conclusion, the experimental data of Fig. 13 prove unequivocally that nitrogen atoms in the $^6S_{5/2}$ metastable state are being detected in the present experiment.

4.4 Time Dependence of the Electric Field Quenching

Figure 14 shows the ratio $R(t, E, E_1)$ vs. t, plotted on semilog paper, corresponding to data of Fig. 12. Here E_1 represents the value of electric field corresponding to the top-most TOF spectra. The channel-by-channel ratio of counts in the respective TOF spectra for a pair of electric fields is taken and plotted. In obtaining these ratios, a uniform background corresponding to the tail of the TOF spectra is subtracted from the actual counts of TOF spectra for all electric fields. This procedure is justified by noting that the average count rate in the "valley" of TOF which precedes the atomic TOF spectrum is only slightly larger than the count rate in the tail of the spectrum.

In Fig. 14, some of the ratio points in earlier channels do not fall on the straight lines of slopes, particularly for larger values of the electric fields. This is due to the contaminations explained in Section 4.2. Therefore, slopes are drawn with respect to latter channels.

As was discussed in detail in Chapter 2, the ratios of electric-field-quenched TOF spectra for atoms in Rydberg levels should always extrapolate to $R < 1$ at $t = 0$ (See Eq. 2.13 and its discussion). In order to obtain an estimate of $R(0, E_2, E_1)$, a computer program was written to calculate $R(t, E_2, E_1)$ for Rydberg-state atoms. In the calculation the known $\gamma_{on} \propto n^{-3}$ (25) was used and it was assumed that

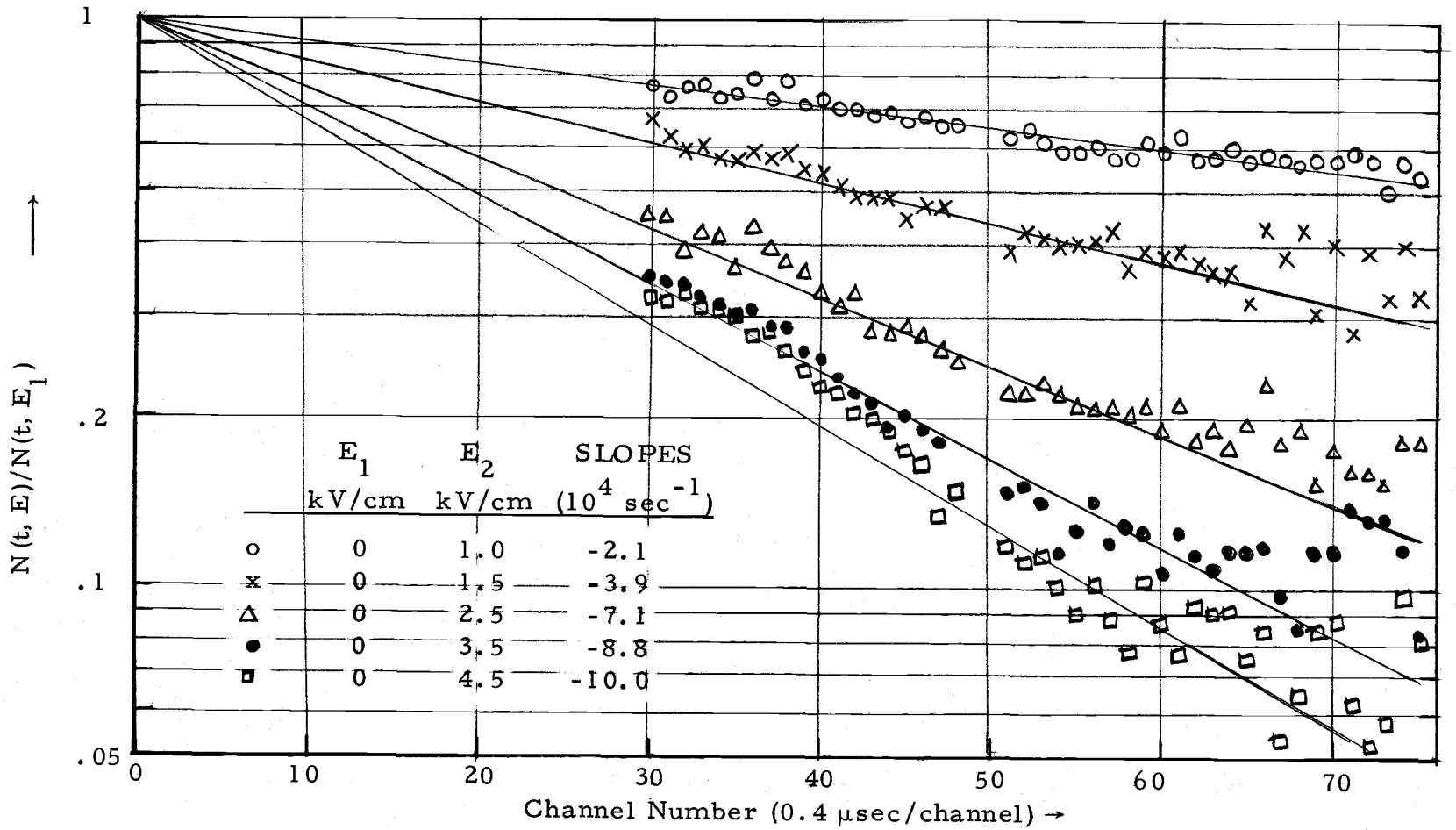

Fig. 14. Quench plots. The channel-by-channel ratios of the TOF spectra shown in Fig. 12. The ratios plotted are those for each of the lower five spectra of Fig. 12 to the uppermost spectrum. For the uppermost spectrum, the quench plates are biased equally; therefore $E_1 = 0$. The slope of the straight lines represents $-(D/L)\ \gamma(E_2)$, because $\gamma(E_1) = 0$ since $E_1 = 0$.

$N_n^{(0)} \propto n^{-3}$, which should be valid if dissociation proceeds via one-electron excitation, because the cross-sections for excitation by electron impact are expected to scale as n^{-3}. The computer plot for Eq. 2.13 was plotted for $n_{min} = 15$, $n_{max} = 30$ and with variable n_c = 27, 24, 20, 17, in the range t = 0 to t = 30 μsec. (For computer program, see Appendix A). The sums were evaluated separately for p- and d-levels, where $\gamma_{np} = 5.26 \times 10^9 \times n^{-3}$ sec^{-1} for the p-level, and $\gamma_{nd} = 1.7 \times 10^9 \times n^{-3}$ sec^{-1} for the d-level (25). It is assumed that for some hypothetical value of minimum electric field, E_1, or in the inevitable fringing fields, Rydberg atoms with n > 30 are quenched by the electric field. Atoms with n < 15 have such a short natural lifetime that they will not contribute to the TOF spectra. Figures 15 and 16 are plots for p- and d- levels respectively. From these plots it is obvious that R < 1 for t = 0, and that, at high fields, $R(0, E_2, E_1) < \frac{1}{2}$. Only p- and d-levels are considered for theoretical ratio plots because the cross-sections for the production of Rydberg state atoms with small orbital angular momentum is much larger than those for atoms in Rydberg states with large orbital angular momentum.

It must also be observed in Figs. 15 and 16 that between 10 and 30 μsec, the fraction of Rydberg state atoms surviving at 3.0 kV/cm electric field is less than 0.01, whereas in Fig. 14, experimentally it is observed that the fraction of metastable atoms surviving in the same time range and at an electric field of 3.5 kV/cm is greater than

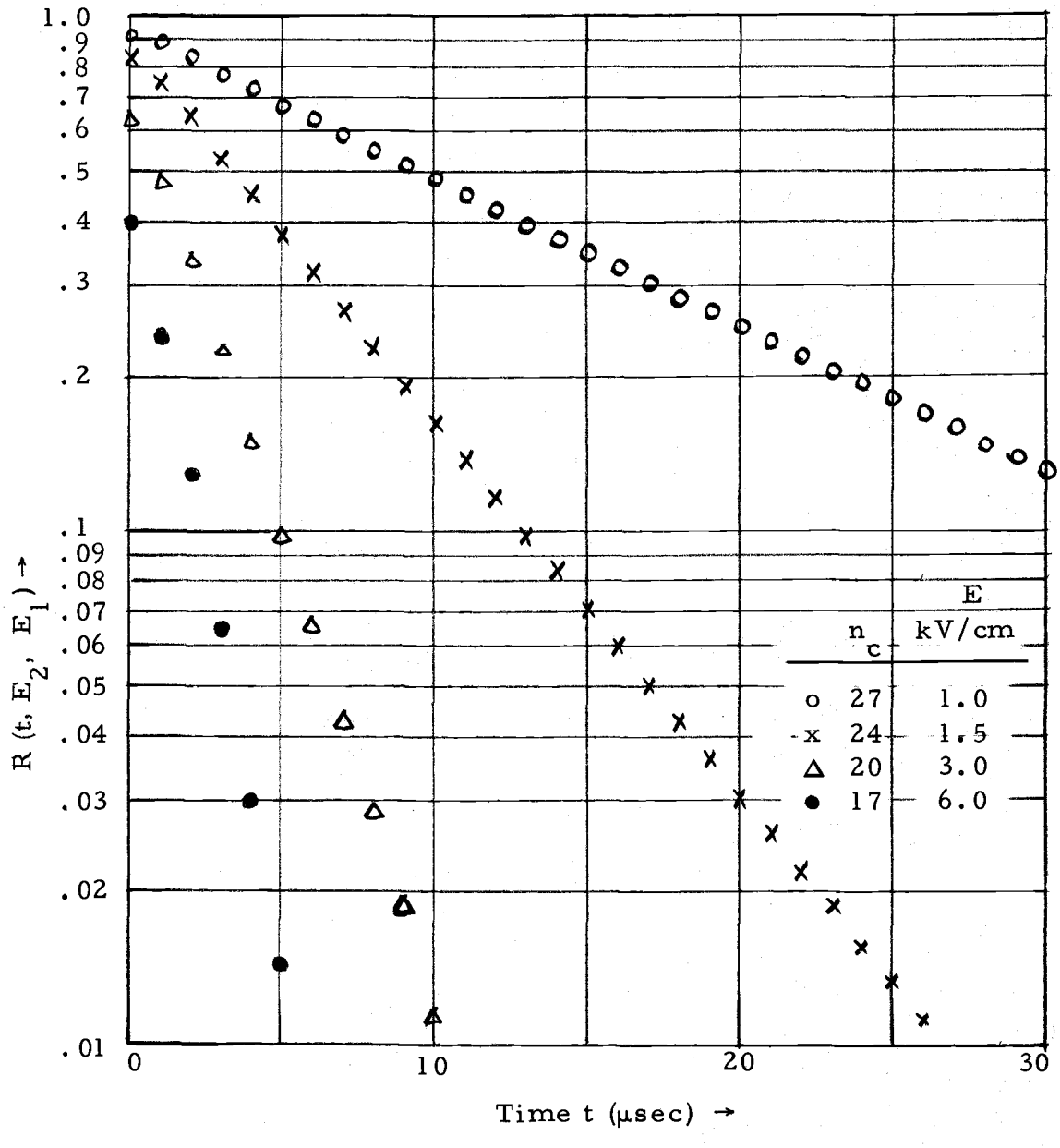

Fig. 15. Computer plots of Eq. 2.13 for p-level Rydberg state atoms for $n_{min} = 15$, $n_{max} = 30$ and different n_c, shown in the legend along with corresponding critical electric field calculated using Fig. 6.

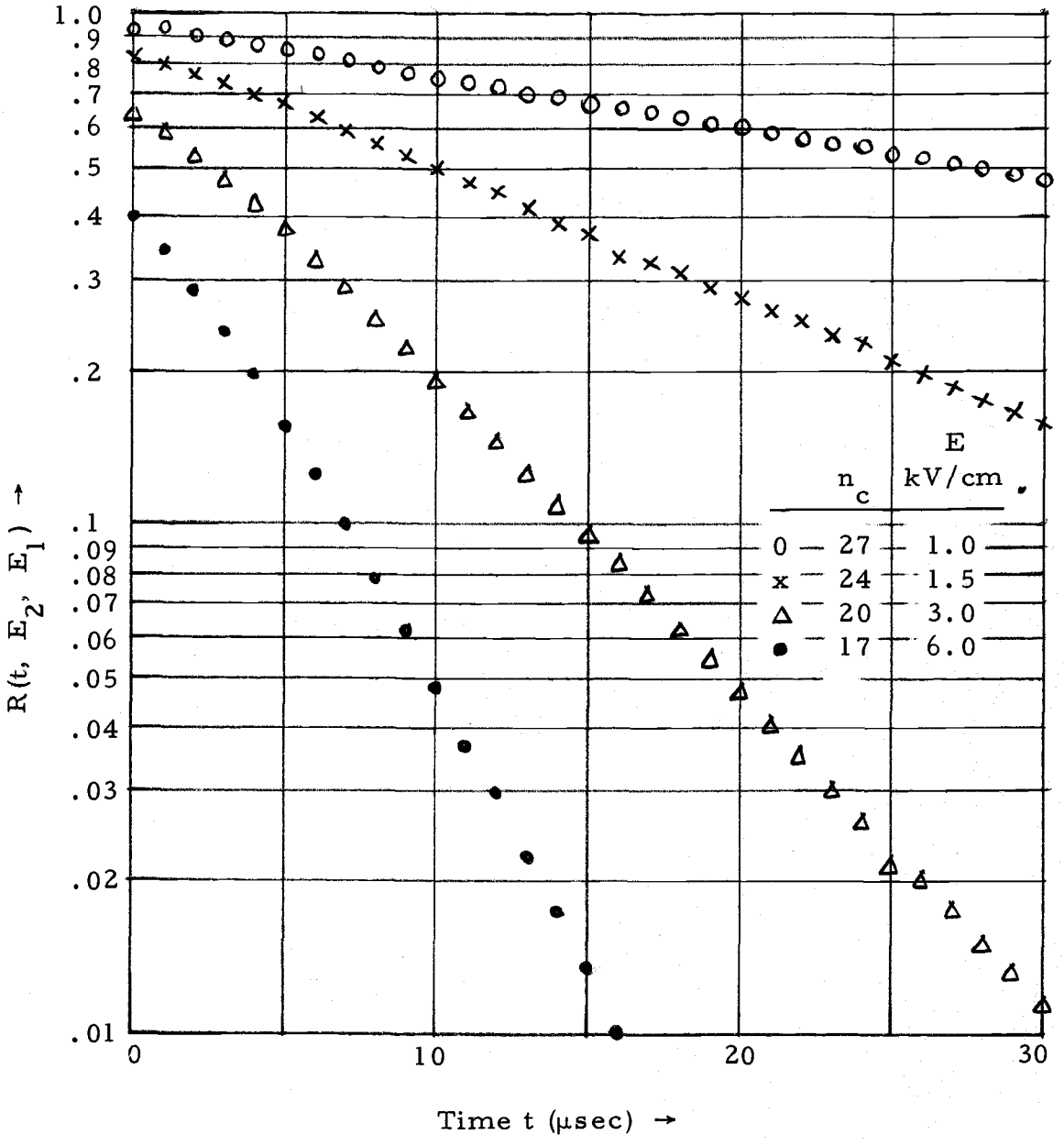

Fig. 16. Computer plots of Eq. 2.13 for d-level Rydberg state atoms for $n_{min} = 15$, $n_{max} = 30$ and different n_c, shown in the legend along with corresponding critical electric field calculated using Fig. 6.

0.12, which is more than a factor of 10 greater. Clearly this is another difference between the experimental results of metastable atoms and the theoretically plotted quench plots for atoms in the Rydberg states.

Thus, the electric field quenching results indicate that the TOF spectra are not due to nitrogen atoms in the Rydberg states and therefore must be due only to nitrogen atoms in the $^6S_{5/2}$ metastable autoionizing state. This conclusion seems to contradict the ideas of Section 2.4D, where it was predicted that atoms in metastable autoionizing states should not be quenched appreciably by the electric fields used in the present experiment. However, these predictions are only qualitative, and it is quite possible that under special circumstances, the decay constant for a metastable autoionizing state may be strongly field dependent even at low fields. This subject is discussed at length in Chapter 5.

In the theory of the electric-field quenching of metastable atoms outlined in Chapter 2, the effects of hyperfine structure were neglected. In fact, since the nitrogen nucleus has a magnetic moment corresponding to a spin of one, the $2s2p^3 3s\ ^6S_{5/2}$ state of nitrogen is split into the three hyperfine levels with total angular momentum quantum numbers F = 7/2, 5/2, 3/2. Since all three of these levels should be populated by the dissociative excitation process, it is to be expected that decay of a beam of these atoms in a dc electric field

should be described by the equation

$$N(t, E) = \sum_{M} N_{M}^{(o)} e^{-\gamma_{M}(E)t} \qquad 4.7$$

where M signifies the electric field angular momentum quantum numbers, i.e., $M = \pm M_F$. Thus, there are nine different terms in the above expression, and the quantity $R(t, E_2, E_1)$ defined in Eq. 2.9 is no longer a linear function of time. However, the conclusion that R = 1 at t = 0 is still valid.

The fact that many of the ratios shown in Fig. 14, lie approximately on a single straight line can be accounted for by assuming that, in the accessible range of TOF, the field-dependent decay is dominated by atoms in electric-field substates of the $^6S_{5/2}$ metastable level having approximately the same lifetime. The fact that the different sets of ratios all extrapolate to R = 1 at t = 0 indicates that atoms in the shortest lived of the electric-field substates contribute significantly to the observed spectra.

Although, the analysis based on the data with prequench grid's electric field on (See Section 4.3), is sufficiently satisfactory to explain that nitrogen atoms in the $^6S_{5/2}$ state are detected in the present experiment, the electric field quenching data (See Section 4.4) are presented as supportive rather than the primary evidence, because of unavoidable difficulties with small amounts of contami-

nations of the TOF spectra, as explained earlier, and which increase with the increasing electric field. It is for this reason that ratios are not taken for the TOF spectra obtained with prequench electric field on, as that causes some contamination in the latter part of the TOF spectrum.

4.5 Lifetime Measurements

During the course of the present work, the natural lifetime of metastable atoms produced by electron bombardment of N_2 molecules, with subsequent excitation and dissociation, was measured at the University of California, Berkeley. This work was supervised by one of the collaborators (C. E. Johnson) of the present experiment, and the experimental results were first reported in the same journal article as the preliminary results for the present experiment (33). The apparatus is similar to the one described in Chapters 2 and 3, but differs in that the TOF spectra are accumulated by the two detectors (instead of one) located at two different positions along the flight path. At the first detector, 68 cm from the electron gun, the flight path is intersected by a 60% transparent metallic mesh, and a second detector is placed at 183 cm from the electron gun, where the flight path is terminated by a solid metallic plate. Details of the apparatus are given elsewhere (33). The principle of measurement and results are given below.

For atoms or molecules in relatively short lived metastable states, the TOF spectra accumulated at the two detectors in the lifetime apparatus differ due to in-flight decay along the flight path between the two detectors. If only one metastable species is present in the atomic beam, its lifetime can be obtained from a comparison of the two spectra. Specifically, the number of atoms, $N_2(t_2)$, detected at the second detector at time t_2, is related to the arrival of $N_1(t_1)$ atoms at the first detector, at the corresponding earlier time, t_1, by the equation

$$N_2(t_2) = C\, N_1(t_1)\, \exp[-(t_2 - t_1)/\tau] \ ,$$

where C is a constant whose value depends upon the relative efficiencies of the two detectors (24), and τ is the natural lifetime of the metastable state. For clarity it is noted that $t_2 - t_1 = (L_2 - L_1)/v$, where $L_2 - L_1$ is the separation of the two detectors and v is the magnitude of an initial velocity, given by $t_1 = L_1/v$, or by $t_2 = L_2/v$. The lifetime, τ, is obtained by evaluating, for the same velocity interval, the point-by-point ratio of the two spectra, and plotting

$$\ell n(N_2/N_1) = \ell n\, C - (t_2 - t_1)/\tau \ , \qquad 4.8$$

as a function of $(t_2 - t_1)$. The slope of the resulting straight line is $-1/\tau$.

A plot of Eq. 4.8, for nitrogen data, is shown in Fig. 17.

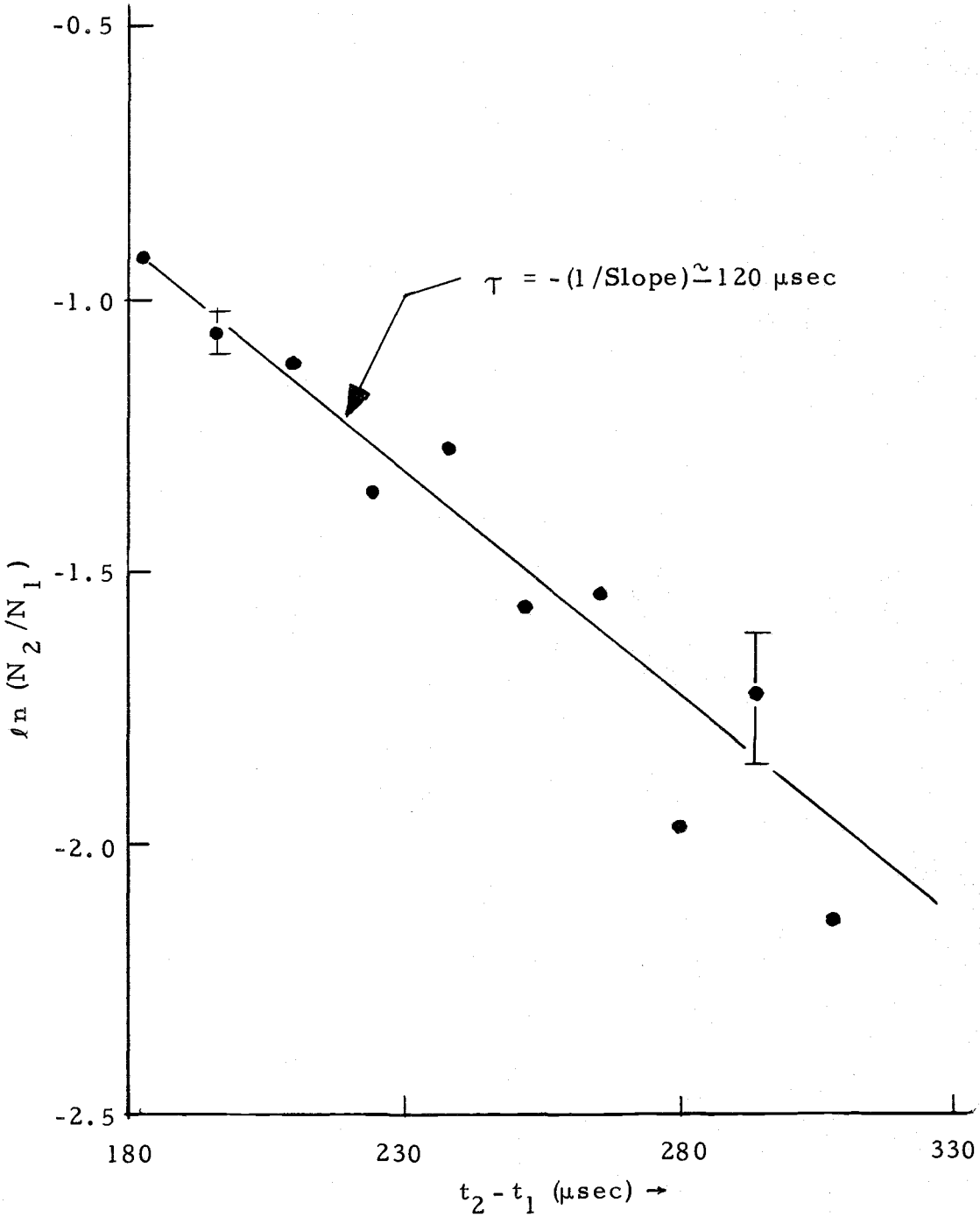

Fig. 17. Decay plot. The point-by-point ratio of the TOF spectra accumulated at the two separate detectors used for a measurement of the lifetime τ.

Although the data are too scattered to allow specification of a single exponential decay, it is clear that the decay is dominated by components with lifetimes of the order of 100 μsec. It will now be shown that because of the effects of collisional quenching in the excitation region, it is highly unlikely that these spectra are due to nitrogen atoms in Rydberg levels. The background gas pressure along the flight path between detectors is always less than 10^{-8} Torr; however, in the excitation region, the operating pressure is typically 5×10^{-6} Torr or higher. Since the distance between the excitation region and the entrance aperture to the flight path is 10 cm, collision quenching of Rydberg atoms can be extremely important in this region. For example, an s-state Rydberg atom with a lifetime of 100 μsec has a principal quantum number $n \simeq 35$; therefore, its gas kinetic mean free path in N_2 at 5×10^{-6} Torr is $\lambda \simeq 3 \times 10^{-2}$ cm. Thus, if collisional quenching cross sections are comparable with or larger than geometrical cross sections, all Rydberg atoms with natural lifetimes greater than 1 μsec have a very low probability for escaping from the excitation region of the lifetime apparatus. On the other hand, metastable atoms with natural lifetimes shorter than 1 μsec must live for approximately 100 lifetimes to reach the nearest detector in this apparatus, and these atoms certainly cannot contribute significantly to the decay curve shown in Fig. 17.

4.6 Conclusion

The TOF spectra of metastable nitrogen atoms produced by dissociative excitation of N_2 molecules by electron bombardment have been presented. It is shown that the spectra are not due to ^4S ground state and ^2D and ^2P metastable states, as the detector used does not have appreciable efficiency for their detection, and this is also confirmed by the lifetime measurement. Of the two remaining alternatives, the $^6S_{5/2}$ metastable state and the Rydberg states for these atoms, the latter are ruled out on the basis of results of electric field quenching and lifetime measurement. It is finally concluded that nitrogen atoms in the $2s2p^3 3s\ ^6S_{5/2}$ metastable autoionizing state are detected in the present experiment.

As mentioned in Chapter 2, nitrogen atoms in Rydberg levels can be produced by dissociative excitation and since the detection scheme used in the present experiment is also suitable for the detection of atoms in Rydberg states, their absence in the TOF spectra needs to be explained. For an electron gun pulse height of 140 V, there is a strong electric field of approximately 4 kV/cm in the excitation region between the cathode and the grids of the electron-gun itself; therefore, any Rydberg atoms with large principal quantum numbers produced in that region are likely to be field ionized as soon as they are produced. DC current measurements show that most

electrons are collected by the control grid and therefore most of the excitation reactions (See Sec. 2.1) take place between the cathode and the control grid. Rydberg atoms with small principal quantum numbers may have such a short lifetime that they may no longer remain in the excited states by the time they reach the detector, and therefore not detected. Additionally, the Rydberg atoms with large principal quantum numbers can also be quenched by collisions with the gas molecules, as the geometrical cross-section varies as n^4. This explains why nitrogen atoms in Rydberg levels are not detected in the present experiment.

5. ANOMALOUS ELECTRIC FIELD QUENCHING OF NITROGEN ATOMS IN THE $2s2p^3 3s\ ^6S_{5/2}$ METASTABLE AUTOIONIZING STATE

5.1 Experimental Results

The evidence of the previous chapter indicates that essentially all of the nitrogen atoms detected in the present experiment at all values of the applied electric field, populate the $^6S_{5/2}$ metastable state; and, since there is substantial quenching even at very low electric fields, the observed electric field quenching of the TOF spectra is regarded as somewhat anomalous. In Fig. 19, approximately 75% of the metastable atoms are quenched at a field strength of 4.5 kV/cm. In contrast, the expected quenching, by comparison with electric field quenching of alkali atoms in metastable autoionizing states (1), is only approximately 1%. To study this problem further, it is assumed that at small values of TOF, the spectrum is dominated by atoms in a single state, or electric field substate. Thus the theory of electric field quenching developed in Chapter 2, can be applied to the data of Fig. 12.

With the assumption of a single decay constant, the slopes of the quench plots shown in Fig. 14 are equal to $-\frac{D}{L}[\gamma(E) - \gamma(E_1)]$ (see Eq. 2.9). In order to understand the functional dependence of $\gamma(E)$ on E, the values of the slope $\frac{D}{L}[\gamma(E) - \gamma(E_1)]$ were plotted

against $\sqrt{E}$, E, and E^2, and it was found that the data best satisfy the linear relation. One such plot for the data of Fig. 12 and the corresponding quench plots in Fig. 14 is shown by the circles in Fig. 18. For $E = E_1$, $\gamma(E) = \gamma(E_1)$, and, therefore, the slope is equal to zero. In Fig. 18, for the data represented by the circles (o), $E_1 = 0$, and, therefore, the line passes through the origin. For the crosses (x), (which are obtained from additional data very similar to those shown in Fig. 12), $E_1 = 0.3$ kV/cm, and, for this reason $\gamma(E) = \gamma(E_1) = 0$ when $E = 0.3$ kV/cm.

The power dependence of $\gamma(E)$ on E can be further verified by plotting $\gamma(E)$ vs. E on log-log paper. Assuming $\gamma(E) = k E^n$, $\ell n\, \gamma(E) = \ell n\, k + n \ell n\, E$. Thus the slope of the line $\gamma(E)$ vs. E, plotted on log-log paper, gives the value of n. Figure 19 shows such plots for the data presented in Fig. 18. As is noted on the figure, the experimental values of n are 1.10 ± 0.04 and 1.08 ± 0.06 for the two sets of data. From the average value $n = 1.09 \pm 0.07$ it is concluded that $\gamma(E)$ varies very nearly linearly with E, i.e., $\gamma(E) = kE$. In Fig. 18, the slope of the line is equal to (D/L)k, from which the average value of k is $(6.4 \pm .5) \times 10^{-4}$ $sec^{-1}/(kV/cm)$.

During the early stages of the present experiment, the observed linear dependence of $\gamma(E)$ on E was considered unphysical, because a straightforward calculation using first order perturbation theory yields $\gamma(E) \propto E^2$ (20, 37). The experiment was therefore repeated

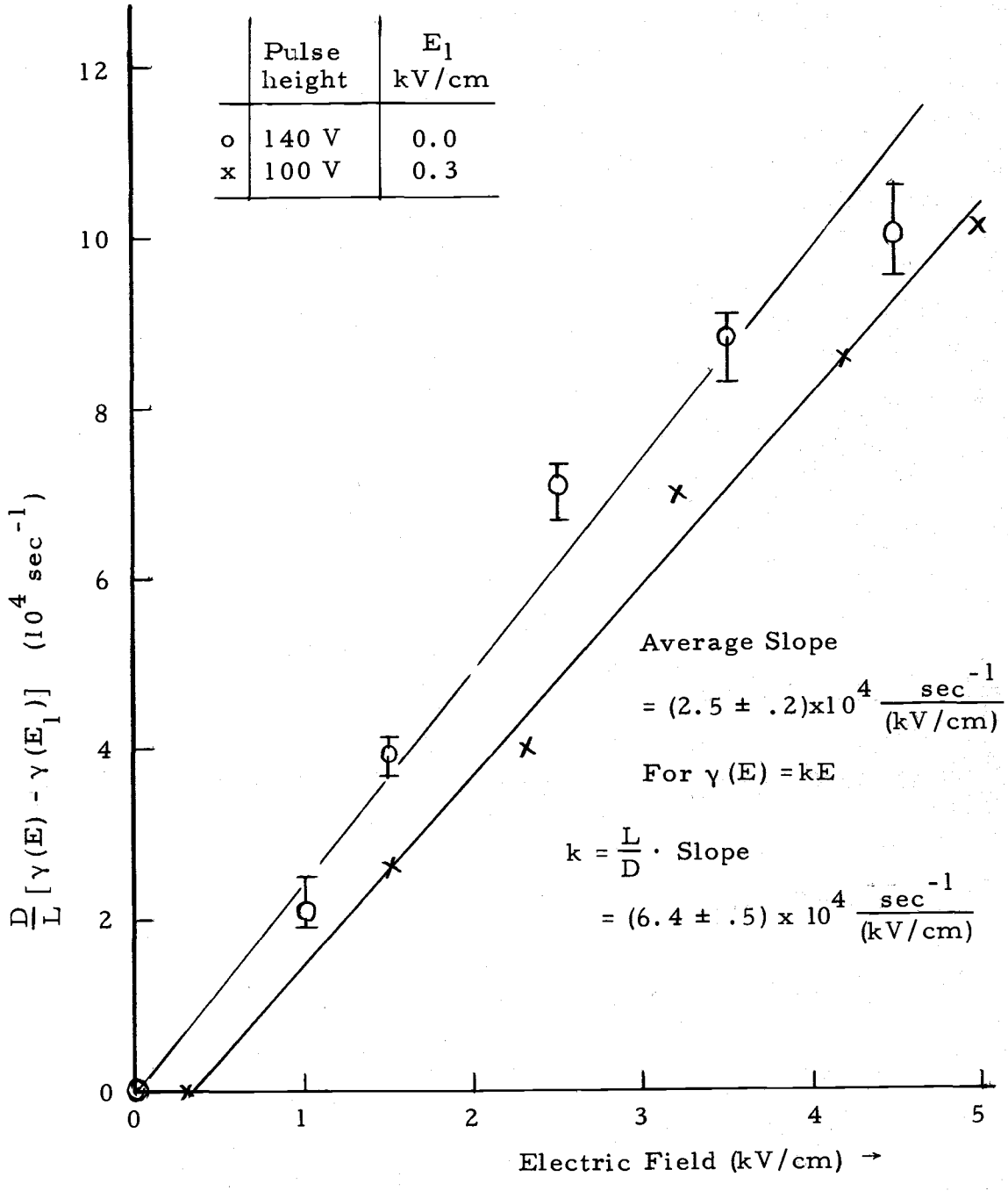

Fig. 18. Dependence of the measured electric field dependent decay rates on the quenching electric field using Eq. 2.9. The open circles (o) represent decay rates from Fig. 14 for the TOF spectra of Fig. 12 and the crosses (x) represent decay rates from additional data at a different electron gun pulse height and a different E_1 field.

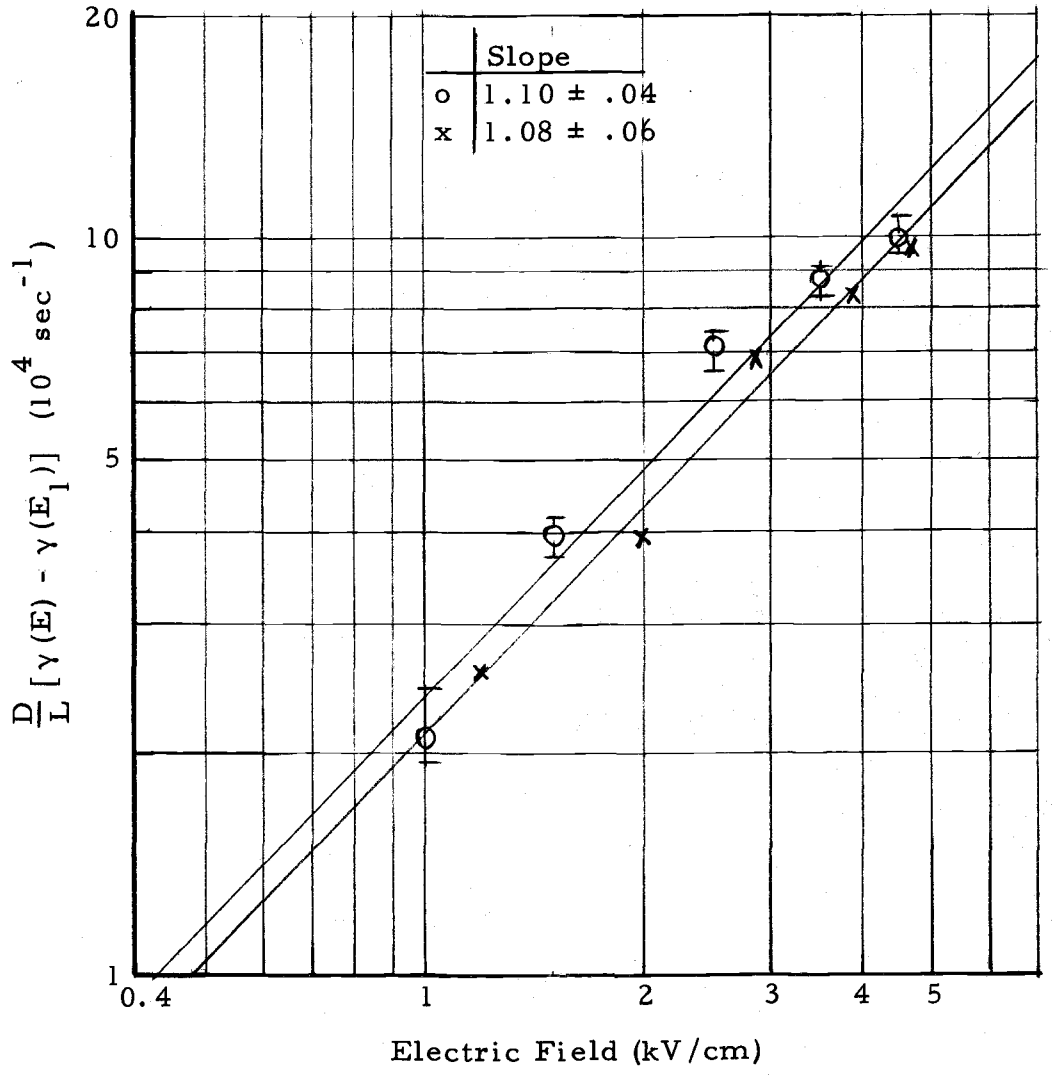

Fig. 19. Log-log plot of the measured electric field dependent decay rates vs quenching electric field showing power dependence of $(D/L)\gamma(E)$ on E. The slope of the straight lines gives the power of E in the relation $\gamma(E) = kE^n$.

several times, using different pressures, different target materials (replacing the Cu-target by a stainless steel plate), different magnetic fields, etc. Under all circumstances, for the range of electric field strengths used in the present experiment, it is found that the experimental data best satisfy the linear relation between $\gamma(E)$ and E.

5.2 Theory of Electric Field Quenching of Nitrogen Atoms in the $2s2p^3 3s\ ^6S_{5/2}$ Metastable Autoionizing State

Because of the relative ease with which nitrogen atoms in the $^6S_{5/2}$ metastable state are quenched in an applied electric field, and because of the non-quadratic dependence of $\gamma(E)$ vs E, it is necessary to propose that the $^6S_{5/2}$ metastable state has some very special or peculiar properties. It is proposed here that instead of lying at 17.2 eV above the ground state as predicted (see Fig. 1), the $^6S_{5/2}$ metastable state is nearly degenerate with the ^1D metastable state of N^+, and that it is mixed strongly with the $2s^2 2p^2(^1D)n\ell$ Rydberg states. This mixing of the $^6S_{5/2}$ metastable state with $2p^2(^1D)n\ell$ Rydberg states is due to internal spin-spin interactions and is present even in the absence of an external electric field. Considering all possible values of n, there are an infinite number of states available for mixing. Even with such strong mixing, the $^6S_{5/2}$ state should be metastable in the absence of any external electric field, because the Rydberg states themselves have long natural lifetimes. When an

electric field is applied, the wave functions for all Rydberg states with principal quantum number $n \geq n_c$ (see Eq. 2.11) become continuum wave functions because of the field ionization effect. As is explained in Section 2.4B, if these states with $n > n_c$ are viewed as decaying states, then, qualitatively, the effect of the electric field is to increase their decay rate by several orders of magnitude. Thus, the hypothesis proposed here is that the electric field quenching of the $^6S_{5/2}$ metastable state is due primarily to the effects of field ionization upon the wave functions of certain nearby Rydberg states. It will now be shown on the basis of these considerations that the electric field dependent decay constant can vary other than quadratically with the applied electric field, and a mechanism is suggested which could possibly give the observed nearly linear dependence of $\gamma(E)$ on E.

In the absence of an external electric field, the wave function of the metastable state resulting from the mixing of the $^6S_{5/2}$ state and $2s^2 2p^2(^1D)n\ell$ Rydberg states by the spin-spin interaction can be written as

$$|\psi> = |^6S_{5/2}> + \sum_n \varepsilon_n |2s^2 2p^2(^1D)n\ell> \quad , \qquad 5.1$$

where the coefficient of mixing ε_n is given by

$$\varepsilon_n = \frac{<2s^2 2p^2(^1D)n\ell| H' |2s2p^3 3s\ ^6S_{5/2}>}{E(^6S) - E(n\ell)} \qquad 5.2$$

Here H' is the spin-spin interaction operator. After expansion of H' and assuming that all angular dependent integrals have been calculated, which mostly give selection rules and coefficients of the order of unity, the radial part of the matrix element is of the form

$$<2s^2 2p^2\, n\ell \left| \frac{1}{r_{ij}^3} \right| 2s2p^3 3s>. \qquad 5.3$$

This matrix element scales as $1/n^{3/2}$, therefore, the probability of finding the metastable atom in the Rydberg state $(n\ell)$, is proportional to $1/n^3$, i.e.,

$$\left| \varepsilon_n \right|^2 = C/n^3 \ , \qquad 5.4$$

where C is a constant of proportionality. This expression is valid only if it is assumed that $E(^6S_{5/2}) \neq E(n\ell)$, for every n and ℓ.

In order to derive a relation between $\gamma(E)$ and E for atoms in the $^6S_{5/2}$ metastable state, let $\Gamma_{Stark}(n)$ be the electric field ionization rate of the Rydberg States with $n \geq n_c$. Then the decay rate in the electric field of atoms in the metastable state $|\psi>$ can be written as

$$\gamma(E) = \sum_{n_c(E)}^{\infty} \left| \varepsilon_n \right|^2 \Gamma_{Stark}(n) \ , \qquad 5.5$$

where summation is done for Rydberg states which lie above the barrier because the ionization rates in the electric field of all other

Rydberg states is comparatively very small (see Section 2.4B).

The electric field ionization rate $\Gamma_{Stark}(n)$ for Rydberg states with energy greater than that of the top of the barrier (Fig. 5), i.e., with $n \geq n_c$, have not been calculated quantum mechanically. Classically, the time required for ionization in the electric field of atoms in such states is of the order of the vibrational period of the motion of an electron in the atom (26), i.e., the ionization rate is of the order of the Bohr frequency of the corresponding Rydberg state. Therefore,

$$\Gamma_{Stark}(n) \simeq \nu_B/n^3 , \qquad 5.6$$

where ν_B is the Bohr frequency for n = 1. Using Eq. 5.4, 5.7 and 5.6,

$$\gamma(E) \simeq \sum_{n_c}^{\infty} \frac{C}{n^3} \cdot \frac{\nu_B}{n^3} \cdot \frac{1}{n_c^5} , \qquad 5.7$$

and using Eq. 2.11,

$$\gamma(E) \propto E^{5/4} . \qquad 5.8$$

Thus, it is shown that the electric field dependent decay rate of atoms in the $^6S_{5/2}$ metastable state can have a power dependence on E different than quadratic.

Equation 5.5 is obtained by considering an incoherent sum of the wave functions of Rydberg states mixed with the $^6S_{5/2}$ state. For a more precise theory, it is proposed that the wave function of Rydberg states above the barrier in the presence of the electric field

be calculated. Using this wave function and the wave function of the $^6S_{5/2}$ state, and considering spin-spin interaction between the two, a new wave function of a metastable state $|\psi>$ can be obtained, including the phase factors in the relation 5.1. The current density can then be obtained by the relation (20),

$$\vec{j} = \frac{\hbar}{2mi} [\psi^* \nabla\psi - \psi\nabla\psi^*],$$

and the transition rate using the relation

$$\gamma(E) = \int \vec{j} \cdot d\vec{A}$$

It is hoped that this technique will give the linear dependence of $\gamma(E)$ on E. The theoretical calculation of the wave functions above the barrier in the presence of the electric field and their mixing with the wave function of the $^6S_{5/2}$ metastable autoionizing state seems to be a formidable task. It is certainly beyond the scope of the present work, and is, therefore, left as an unsolved problem.

6. SUGGESTED ADDITIONAL EXPERIMENTS

The present work does not exhaust the possibilities for experimental study of metastable nitrogen atoms produced by dissociative excitation. Since it has been shown that nitrogen atoms in $2s2p^3 3s\ ^6S_{5/2}$ metastable autoionizing state exist and can be easily produced in the laboratory, their other properties can now be studied. Further information about the $^6S_{5/2}$ metastable atoms can be obtained by using atomic beam techniques. Some of them are described below.

6.1 Magnetic Deflection of Nitrogen Atoms in the $^6S_{5/2}$ State

The magnetic moment of atoms can be determined by the Stern-Gerlach effect. Since nitrogen atoms in the $^6S_{5/2}$ metastable state can be produced by dissociative excitation, an experiment can be designed combining the time-of-flight technique and the Stern-Gerlach effect to obtain more information about nitrogen atoms in $^6S_{5/2}$ metastable state.

An atom with mass M and effective magnetic moment μ_{eff} will be deflected by an inhomogeneous magnetic field, the deflection d being given by (34)

$$d = \tfrac{1}{2} \frac{\mu_{eff}}{M} \frac{dH}{dz} t^2 , \qquad 6.1$$

where t is the time required for the atom to traverse the inhomogene-

ous magnetic field, $\frac{dH}{dz}$ is the gradient of the magnetic field perpendicular to the direction of flight path. If nuclear spin is neglected μ_{eff} is given by

$$\mu_{eff} = g_J \, m_J \, \mu_B , \qquad 6.2$$

where μ_B is the Bohr magneton, equal to 9.27×10^{-21} erg/gauss, m_J is the magnetic quantum number and g_J is the Landé g factor. For the $^6S_{5/2}$ state, $g_J = 2$, and m_J can take values $\pm \frac{5}{2}$, $\pm \frac{3}{2}$ or $\pm \frac{1}{2}$. Therefore, μ_{eff} can be $\pm 5 \mu_B$, $\pm 3 \mu_B$ or $\pm 1 \mu_B$. By measuring deflection, magnetic field gradient and time spent in the magnetic field, the effective magnetic moment can be calculated. It is expected that the beam must split into six different portions when an inhomogeneous magnetic field is on, as compared to one beam in the absence of the magnetic field. Also, since the different magnetic sublevels will be seen to have different lifetimes, it may not be possible to find all the components in a given experiment, because the lifetime of some of the components may be much smaller than the time-of-flight.

Thus, by precisely measuring the magnetic moment, the state of the atoms can be identified. It should be mentioned, though, that the speed of nitrogen atoms in the $^6S_{5/2}$ state obtained by dissociative excitation is quite large compared to the thermal velocities of the atoms or molecules generally used in a Stern-Gerlach type experiment. Therefore, either a very large magnetic field gradient is

required or the deflection will be very small. To resolve the different components, a very fine beam of atoms will be needed.

6.2 Radiofrequency Spectroscopy of Nitrogen Atoms in the $^6S_{5/2}$ Metastable State

Another precise method to measure the atomic magnetic moments or to identify the state of an atom is by an atomic beam resonance method. In this method, the atoms are in a uniform magnetic field, and radio-frequency transitions are induced between the different energy levels of the atoms. Some considerations which apply for the $^6S_{5/2}$ metastable state of nitrogen are given below.

The nuclear angular momentum quantum number for N^{14} nucleus is I = 1. Considering the coupling between the nuclear angular momentum and total electronic angular momentum, for J = 5/2, F can have 7/2, 5/2, 3/2 as possible values. Thus, due to hfs, the energy level corresponding to J = 5/2 is split into three levels. In the presence of external magnetic field, each of the F levels will be further split into magnetic sublevels. In all, for J = 5/2, there will be 18 magnetic sublevels. Due to internal magnetic interactions, for which the selection rules are given in Table I (page 5), the F = 7/2 level can couple to a total of eight states, including autoionizing states of the same configuration and those of the continuum. Similarly, F = 5/2 state can couple to a total of 16 states and F = 3/2 to seven states.

The autoionizing rate of a state depends not only on the number of the autoionizing or continuum states with which a state couples, but also on the energy separations and matrix elements of the interaction Hamiltonian between interacting states. The number of states to which a given state is coupled gives an indication of its rate of autoionization. Thus, F = 7/2, 5/2, and 3/2 levels may have different lifetimes; i.e., there can be differential metastability. From the above, the F = 7/2 level seems to be longest lived out of the three levels. In the presence of an external magnetic field, states are mixed according to the selection rule $\Delta F = \pm 1$, and $\Delta M_F = 0$. Thus, for F = 7/2, in the presence of a magnetic field, out of eight magnetic sublevels $m_F = \pm 7/2, \pm 5/2, \pm 3/2, \pm 1/2$, six sublevels ($m_F = \pm 5/2, \pm 3/2, \pm 1/2$) will be mixed with those of F = 5/2 and therefore will have shorter lifetime as compared to the lifetime of $m_F = \pm 7/2$. Therefore, in the presence of magnetic field, a population difference between atoms with $m_F = \pm 7/2$ and $m_F = \pm 5/2$ can be produced. Since the transition probabilities between a pair of states for upward (absorption) and downward (stimulated emission) transitions, excited by a r.f. field of given frequency and intensity are identical (40, p. 119), it is important to have a population difference to begin with so as to have a detectable effect at resonance in the signal due to metastable atoms. Thus, r.f. transitions can be induced between levels with $m_F = \pm 7/2$ and $m_F = \pm 5/2$ and at resonance the

signal of $m_F = \pm 7/2$ must decrease, and the effective magnetic moment or g_F factor can be measured.

The energy separation between adjacent magnetic sublevels in the presence of external magnetic field of magnitude B is given by

$$\Delta E = g_F \mu_B B$$

At resonance, $h\nu = g_F \mu_B B$, from which g_F can be calculated by measuring the frequency ν and magnetic field B at which resonance takes place. On the other hand, theoretically (16),

$$g_F = g_J \cdot \frac{F(F+1) + J(J+1) - I(I+1)}{2F(F+1)}$$

and

$$g_J = 1 + \frac{J(J+1) - L(L+1) + S(S+1)}{2J(J+1)}$$

For $^6S_{5/2}$, $g_J = 2$ and therefore, for $F = 7/2$, $g_F = 10/7$, and at resonance one expects the relation

$$\nu = 1.98\left(\frac{\text{MHz}}{\text{Gauss}}\right) \cdot B(\text{Gauss})$$

Generally, frequency is kept fixed and the magnetic field is varied to observe resonance.

Based on the above ideas, an effort was made by the author to observe r.f. resonance, but it was not successful possibly due to an insufficient population difference between atoms with $m_F = \pm 7/2$ and

$m_F = \pm 5/2$ levels.

A preliminary investigation was also done by Incesu (34), but no resonance was seen, possibly due to too large a size (2 meters) of the apparatus resulting in weak signal at the detector, and large noise in his apparatus. Therefore, a very careful designing of the apparatus is required.

BIBLIOGRAPHY

1. Feldman, P. and R. Novick. Auto-Ionizing States in the Alkali Atoms with Microsecond Lifetimes. Physical Review 160:143-158. 1967.

2. Levitt, M., R. Novick and P. D. Feldman. Determination of Energies and Lifetimes of the Metastable Auto-Ionizing $(1s2s2p)^4P$ States of Li^6 and Li^7 by a Zeeman-Quenching Technique. Physical Review 3:130-146. 1971.

3. Manson, S. T. Calculation of Auto-Ionization Rates. Physical Review 145: 35-40. 1966.

4. Manson, S. T. Theoretical Considerations for Auto-Ionizing States with Microsecond Lifetimes. Physical Review A 3:147-153. 1971.

5. Nicolaides, C. A. Theoretical Approach to the Calculation of Energies and Widths of Resonant (Autoionizing) States in Many-Electron Atoms. Physical Review A 6: 2078-2092. 1972.

6. Fano, U. Effects of Configuration Interaction on Intensities and Phase Shifts. Physical Review. 124: 1866-1878. 1961.

7. Dehmer, P. M., J. Berkowitz and W. A. Chupka. Photoionization of Atomic Nitrogen. The Journal of Chemical Physics 60: 2676-2679. 1974.

8. Dehmer, P. M., J. Berkowitz and W. A. Chupka. Photoionization of Atomic Oxygen from 920 to 650 Å. The Journal of Chemical Physics 59: 5777-5786. 1973.

9. Herzberg, Gerhard. Atomic Spectra and Atomic Structure. New York, Dover Publications, 1944. 257 p.

10. Wright, A. N. and C. A. Winkler. Active Nitrogen. New York, Academic Press, 1968. 602 p.

11. Moore, Charlotte. Atomic Energy Levels. Vol. I. Washington, D.C., 1952. 227 p. (National Bureau of Standards. Circular 467)

12. Innes, F. R. and O. Oldenberg. Metastable Atoms and the Auroral Afterglow of Nitrogen. The Journal of Chemical Physics 37: 2427-2428. 1962.

13. Oldenberg, O. A Theory of the Auroral Afterglow of Nitrogen. Physical Sciences Research Papers Report No. 323, Office of Aerospace Research, United States Air Force, 1967 (Unpublished).

14. Prag, A. B. and K. C. Clark. Excitation Mechanism for the Nitrogen Pink Afterglow. The Journal of Chemical Physics 39: 799-805. 1963.

15. Prag, A. B. and K. C. Clark. Estimated Energy of the Metastable Sextet Atom of Nitrogen. The Journal of Chemical Physics 38: 2305-2306. 1963.

16. Condon, E. U. and G. H. Shortley. The Theory of Atomic Spectra. Cambridge, The University Press, 1964. 441 p.

17. Mizushima, Masataka. Quantum Mechanics of Atomic Spectra and Atomic Structure. New York, W. A. Benjamin, Inc., 1970. 419 p.

18. White, H. E. Introduction to Atomic Spectra. New York, McGraw Hill Book Co., Inc. 1934. 457 p.

19. Kuhn, H. G. Atomic Spectra. New York, Academic Press, 1969. 472 p.

20. Merzbacher, Eugene. Quantum Mechanics. New York, John Wiley and Sons, Inc., 1961. 544 p.

21. Pegg, D. J., P. M. Griffin and I. A. Sellin. Metastable States of Highly Excited Heavy Ions. In: Atomic Physics 3, ed. by S. J. Smith and G. K. Walters. Plenum Press, New York-London, 1973. p. 327-337.

22. Freund, Robert S. Dissociation by Electron Impact of Oxygen into Metastable Quintet and Long-Lived High-Rydberg Atoms. The Journal of Chemical Physics 54: 3125-3141. 1971.

23. Gilmore, F. R. Potential Energy Curves for N_2, NO, O_2 and corresponding ions. Journal of Quantitative Spectroscopy and Radiative Transfer 5: 369-390. 1965.

24. Smyth, K. C., J. A. Schiavone and Robert S. Freund. Dissociative Excitation of N_2 by Electron Impact: Translational Spectroscopy of Long-lived High-Rydberg Fragment Atoms. The Journal of Chemical Physics 59: 5225-5241. 1973.

25. Bethe, H. A. and E. E. Salpeter. Quantum Mechanics of One- and Two-Electron Atoms. New York, Academic Press, 1957. 368 p.

26. Fedorenko, N. V., V. A. Ankudinov and R. N. Il'in. Lorentz Ionization of Highly Excited Hydrogen Atoms. Zhurnal Tekhnicheskoi Fiziki 35: 585-604. 1965. (Translated in Soviet Physics-Technical Physics 10: 461-476. 1965.)

27. Hughes, Vernon and H. L. Schultz. Atomic and Electron Physics, Vol. 4, Part A. In: Methods of Experimental Physics Series. New York Academic Press, 1967. 515 p.

28. Chaplik, A. V. Ionization of Highly Excited Atoms Near a Metallic Surface. Zhurnal Eksperimental 'noii Teoreticheskoi Fiziki 54: 332-338. 1968. (Translated in Soviet Physics JETP 27: 178-181. 1968.)

29. Kupriyanov, S. E. Ionization of Highly Excited Atoms and Ions of Noble Gases in an Electric Field and near a Metallic Surface. Zhurnal Eksperimental'noii Teoreticheskoi Fiziki Prisma 5: 245-248. 1967. (Tranlated in Soviet Physics JETP Letters 5: 197-199. 1967.)

30. Morack, John Ludwig. Measured Lifetimes for the First Excited $J=1$ ($^3P_1$) level in Argon and Krypton. Doctoral dissertation. Corvallis, Oregon State University, 1969. 94 numb. leaves.

31. Rice, M. H. and R. H. Good, Jr. Stark Effect in Hydrogen. Journal of the Optical Society of America 52: 239-246. 1962.

32. Bailey, D. S., J. R. Hiskes and A. C. Riviere. Electric Field Ionization Probabilities for the Hydrogen Atom. Nuclear Fusion 5: 41-46. 1965.

33. Fairchild, C. E., H. P. Garg and C. E. Johnson. Detection of Nitrogen Atoms in the $2s2p^3 3s\ ^6S_{5/2}$ Metastable Autoionizing State. Physical Review A 8: 796-804. 1973.

34. Incesu, Tuncay. Studies of the Dissociation Fragments of N_2 and the g_J Measurement of Metastable $^5S_2$ Atomic Oxygen. Ph.D. thesis. Berkeley, University of California, 1974. 139 numb. leaves.

35. Feldman, P. and R. Novick. Evidence for a Metastable Sextet State in Nitrogen. Bulletin of the American Physical Society (2), 10: 455. 1965.

36. Il'in, R. N. Ionization of Excited Atomic Particles by Electric Fields. In: Atomic Physics 3, ed. by S. J. Smith and G. K. Walters. Plenum Press, New York, 1973. p. 309-326.

37. Johnson, C. E. Quenching of the 2^1S_0 Metastable State of the Helium by an Electric Field. Physical Review A 7: 872-880. 1973.

38. Bederson, Benjamin and W. L. Fite. Atomic and Electron Physics, Vol. 7, Part A. In: Methods of Experimental Physics Series. New York, Academic Press, 1968. 506 p.

39. Rice, M. H. Theory of the Stark Effect in Hydrogen at High Fields. Doctoral Dissertation. Ames, Iowa State College, 1958. 65 numb. leaves.

40. Hughes, Vernon and H. L. Schultz. Atomic and Electron Physics, Vol. 4, Part B. In: Methods of Experimental Physics Series. New York, Academic Press, 1967. 345 p.

APPENDIX

APPENDIX

Computer program for calculating the ratios defined by Eq. 2.11 and plotted in Figs. 15 and 16.

For p-level $C1 = 5.0 \times 10^3$

For d-level $C1 = 1.7 \times 10^3$

$N1 = n_{min}$, $N2 = n_c$, $N3 = n_{max}$

```
00001:          PROGRAM RATIO
00002:       11 N1=TTYIN(4HN1= )
00003:          IF(N1.EQ.0)GO TO 200
00004:          N2=TTYIN(4HN2= )
00005:          N3=TTYIN(4HN3= )
00006:          C1=TTYIN(4HC1= )
00007:          DO 100 I=0, 300, 10
00008:          T=I/10.
00009:          S=0.
00010:          DO 50 J=N1, N2
00011:          C=J**3
00012:          E1=-C1*T/C
00013:          Z=EXP(E1)/C
00014:          S=S+Z
00015:50        CONTINUE
00016:          X=S
00017:          NA=N2+1
00018:          DO 75 J=NA, N3
00019:          C=J**3
00020:          E1=-C1*T/C
00021:          Z=EXP(E1)/C
00022:          S=S+Z
00023:75        CONTINUE
00024:          Y=S
00025:          R=X/Y
00026:          WRITE(61, 1) R, T
00027:1         FORMAT(' 'F8.4, 3X, F4.1)
00028:100       CONTINUE
00029:          GO TO 11
00030:200       CALL EXIT
00031:          END
```